

Experimental and numerical investigation on the optical and thermal performance of solar parabolic dish and corrugated spiral cavity receiver

Pavlovic, Sasa; Daabo, Ahmed M.; Bellos, Evangelos; Stefanovic, Velimir; Mahmoud, Saad; Al-dadah, Raya K.

DOI:

[10.1016/j.jclepro.2017.02.201](https://doi.org/10.1016/j.jclepro.2017.02.201)

License:

Creative Commons: Attribution-NonCommercial-NoDerivs (CC BY-NC-ND)

Document Version

Peer reviewed version

Citation for published version (Harvard):

Pavlovic, S, Daabo, AM, Bellos, E, Stefanovic, V, Mahmoud, S & Al-dadah, RK 2017, 'Experimental and numerical investigation on the optical and thermal performance of solar parabolic dish and corrugated spiral cavity receiver', *Journal of Cleaner Production*, vol. 150, pp. 75-92. <https://doi.org/10.1016/j.jclepro.2017.02.201>

[Link to publication on Research at Birmingham portal](#)

General rights

Unless a licence is specified above, all rights (including copyright and moral rights) in this document are retained by the authors and/or the copyright holders. The express permission of the copyright holder must be obtained for any use of this material other than for purposes permitted by law.

- Users may freely distribute the URL that is used to identify this publication.
- Users may download and/or print one copy of the publication from the University of Birmingham research portal for the purpose of private study or non-commercial research.
- User may use extracts from the document in line with the concept of 'fair dealing' under the Copyright, Designs and Patents Act 1988 (?)
- Users may not further distribute the material nor use it for the purposes of commercial gain.

Where a licence is displayed above, please note the terms and conditions of the licence govern your use of this document.

When citing, please reference the published version.

Take down policy

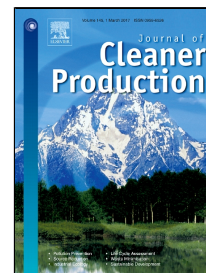
While the University of Birmingham exercises care and attention in making items available there are rare occasions when an item has been uploaded in error or has been deemed to be commercially or otherwise sensitive.

If you believe that this is the case for this document, please contact UBIRA@lists.bham.ac.uk providing details and we will remove access to the work immediately and investigate.

Accepted Manuscript

Experimental and Numerical Investigation on the Optical and Thermal Performance of Solar Parabolic Dish and Corrugated Spiral Cavity Receiver

Sasa Pavlovic, Ahmed M. Daabo, Evangelos Bellos, Velimir Stefanovic, Saad Mahmoud, Raya K. Al- Dadah



PII: S0959-6526(17)30427-4
DOI: 10.1016/j.jclepro.2017.02.201
Reference: JCLP 9127
To appear in: *Journal of Cleaner Production*
Received Date: 29 October 2016
Revised Date: 28 February 2017
Accepted Date: 28 February 2017

Please cite this article as: Sasa Pavlovic, Ahmed M. Daabo, Evangelos Bellos, Velimir Stefanovic, Saad Mahmoud, Raya K. Al- Dadah, Experimental and Numerical Investigation on the Optical and Thermal Performance of Solar Parabolic Dish and Corrugated Spiral Cavity Receiver, *Journal of Cleaner Production* (2017), doi: 10.1016/j.jclepro.2017.02.201

This is a PDF file of an unedited manuscript that has been accepted for publication. As a service to our customers we are providing this early version of the manuscript. The manuscript will undergo copyediting, typesetting, and review of the resulting proof before it is published in its final form. Please note that during the production process errors may be discovered which could affect the content, and all legal disclaimers that apply to the journal pertain.

Highlights:

- Experimental testing of solar prototyping solar dish collector was conducted.
- Thermal efficiency and exergetic efficiency of the different working fluids for solar spiral corrugated absorber were determined.
- A numerical model was used for estimating the energetic and exergetic performance of the collector in various operating cases.
- The effect of the helical conical receiver position on optical efficiency was investigated.

Experimental and Numerical Investigation on the Optical and Thermal Performance of Solar Parabolic Dish and Corrugated Spiral Cavity Receiver

Sasa Pavlovic^{a,*}, Ahmed M. Daabo^{b,c}, Evangelos Bellos^d, Velimir Stefanovic^a,
Saad Mahmoud^b, Raya K. Al- Dadah^b

^aDepartment of Energetics and Process technique, Faculty of Mechanical Engineering, University in Niš, Serbia.

^bSchool of Mechanical Engineering University of Birmingham.
Birmingham, B15 2TT; axd434@bham.ac.uk

^cThe University of Mosul, Mechanical Engineering Department, Ninawa, Iraq.

^dNational Technical University of Athens, School of Mechanical Engineering, Athens, Greece.

*Corresponding author: Sasa Pavlovic (saledoca@gmail.com)

Abstract

A low cost solar collector with a dish reflector and spiral absorber is examined in this work. This collector is investigated experimentally and numerically with a developed thermal model in the Engineering Equation Solver (EES). Numerical simulations are performed by the commercial software OptisWorks. The solar ray distribution inside these receiver geometries, including the helical coil used for the heat transfer fluid, was determined using this tool. The final results show that the thermal performance is about 34%, due to the high rate of thermal losses. After validating the numerical model, it is used for investigating the collector for various operating conditions. Three working fluids (Water, Therminol VP-1 and Air) are compared energetically and exergetically for various combinations of volumetric flow rates and operational temperature levels. The results proved that water is the most appropriate working fluid, among those investigated, as it is able to efficiently work at low temperature levels, while the thermal oil is the best at higher temperature values, according to thermal analysis. The exergetic analysis showed that air is the best choice in low temperatures and thermal oil in greater temperatures. Finally, an open receiver of a conical cavity shape with a helical tube was optically investigated, as a second strategy for enhancing the optical performance of the receiver. The results show that an average flux value of about 2.6×10^5 W/m² was absorbed by the helical conical shape with an aperture area of 0.01606 m².

Keywords:

Parabolic concentrator dish, Ray tracing simulation, Experimental analysis, Thermal analysis

1. Introduction

Renewable energy plays an important role in the current continuous increasing energy demand and at the same time too many emissions and greenhouse problems. This incessant request on the energy was one of the main reasons which contributed in expanding the utilization of the solar thermal energy (Sánchez et al. 2016). Moreover, there are many important problems related with the energy domain, as the increasing electricity demand, the high CO₂ emissions and the fossil fuel depletion (Iodice et al. 2016). The use of renewable and alternative energy sources is a sustainable way for substituting the fossil fuel with cheap and abundant energy sources (Daabo et al. 2016a). Solar energy utilization is a basic weapon for facing the energy problems, giving efficient, clean and financially viable solutions (Bellos et al. 2016c).

45 Solar collectors are the devices which capture solar energy and transform it to useful heat,
46 with satisfying efficiency. For low temperature levels up to 100 °C, flat plate collectors are the
47 most usual collector type (Bellos et al. 2016a). For medium temperature levels up to 200 °C,
48 evacuated tube collectors and low quality concentration collector are the most usual collectors
49 (Kalogirou 2004). For high temperature levels, parabolic trough collector, Fresnel collectors
50 and solar dish collectors are the most ideal solution for achieving satisfying results (Pavlović
51 et al. 2016).

52 Solar dish collectors are a reliable solution for operation in medium and high temperature
53 levels. (Abid et al. 2015) compared a solar dish collector with a parabolic trough collector and
54 the final results proved that the dish technology performs better because of the higher
55 concentration ratio which is fully connected with lower thermal losses and higher thermal
56 efficiency. The solar dish concentrators have been used in a great variety of applications for
57 heat and electricity production. The use of solar dish concentrators in gas turbine systems has
58 been intensively studied during the last years. (Mohammadi and Mehrpooya 2016) and (Daabo
59 et al. 2017) investigated and optimized an integrated micro gas turbine with solar dish
60 collectors to be used between the gas preheater and the combustion chamber. (Loni et al.
61 2016) examined the use of a solar dish collector with cavity receiver in an organic Rankine
62 cycle. The followed methodology proved that there is optimum concentration ratio which
63 maximizes the work output and the authors proposed the conduction of detailed optical
64 analysis for determining the optimum receiver dimensions in every design. Also, the use of
65 hybrid solar dish collectors in desalination system has been conducted in literature (Omara and
66 Eltawil 2013). Likewise, the use of pure solar energy to desalinate sea salt water for a
67 domestic application was conducted by (Prado et al. 2016). The conjugation of Stirling heat
68 engines with solar dish plates is a promising technology for producing electricity with high
69 performance but also with high investment cost (Xiao et al. 2017). The main purpose of the
70 recent studies regarding this filed is to reduce the cost of the system and to design collectors
71 with higher optical performance. (Li et al. 2011) utilized a Monte-Carlo ray tracing method for
72 determining the heat flux distribution over the receiver. The results proved that the most
73 uniform heat flux profile can be achieved with a shallow semi-ellipsoidal receiver.

74 The design of the solar dish collector is not well-established, with numerous configurations to
75 be studied and to be suggested. Two main parts of the thermal system are analyzed; the
76 reflector and the receiver. The dish reflector size can be varying a lot, from small dishes (for
77 example 0.5 m² or 1 m²) up to huge systems. (Lovegrove et al. 2011) investigated a 500 m²
78 solar dish concentrator with 380 identical spherical mirror panels. However, this scale is not
79 always achievable. (Cohen and Grossman 2016) studied a great stationary reflector which can
80 be manufactured with low cost. This reflector was similar to a spherical bowl and the absorber
81 was a cylindrical coil painted with flat-black. The absorber is located in a glass cover while
82 vacuum conditions exist there for minimization of the rate of thermal losses. However, the
83 reflector was fixed on specific position which obviously would not be accounted as an
84 efficient system.

85 Other studies have been focused on the receiver investigation in order to compare various
86 possible candidates. (Daabo et al. 2016b) examined, optically, three cavity receiver
87 geometries; cylinder, cone and sphere without inserting helical tube and then in the next study
88 (Daabo et al. 2016c), a helical tube was used inside in order to capture utilize the solar energy
89 with an efficient way. According to the final results, the conical shape is the best choice
90 among the examined cases. Besides, they proved that the optimum reflector geometry is

91 depended on the selected receiver; an interesting result which is useful in the design of
92 innovative solar dish collectors. A parabolic dish concentrator and cavity receiver with quartz
93 glass cover system were presented in the study done by (Cui et al. 2013). A 2-D simulation
94 model for combined natural convection and surface radiation has been developed. The results
95 of simulation showed that compared with the uncovered receiver, the quartz glass cover
96 largely reduces the natural convection and surface radiation heat losses of the cavity receiver.
97 The total heat flux of the covered receiver at an inclination of 0° was only about 36% of that
98 for uncovered receiver. However, neither 3D analysis on the coupled heat transfer process of
99 the cavity receiver nor the heat flux uniformity were conducted. A numerical study on the
100 phase change materials for a vertical cylindrical receiver was examined by (Tao et al. 2013).
101 The feasibility from the techno-economic view point of a 5MWe solar parabolic dish collector
102 field at different areas in India was analysed by (Reddy and Veershetty 2013). Different
103 parameters like percentage of the shadow, spacing between dish collectors and energy yield
104 were numerically investigated. The result showed that there was shadow profile changing
105 with the latitude of (8–35_N). As for the location, their results showed that there are some
106 attractive regions; Direct Normal Irradiance DNI is more than 5 kWh/m² day, in the
107 investigated locations which can be used for power generation using the solar parabolic dish.
108 The analysis of a hybrid cooling and heating integrated with Stirling engine and absorption
109 chiller has been proposed and analyzed by (Mehrpooya et al. 2017).

110 (Przenzak et al. 2016) investigated a solar dish collector, with two optical elements and a
111 curved radiation absorber. This collector is designed for operation in high temperature levels
112 and there is a proper design for achieving this goal. The authors of this work performed a
113 parametric investigation in order to determine the optimum receiver location and the most
114 suitable mass flow rate. (Reddy and Kumar 2009) examined a modified cavity receiver of a
115 solar dish collector and they specifically focused on the natural convection losses of the
116 presented collector. Furthermore, they, experimentally, includes a detailed optical analysis of
117 this receiver in (Reddy et al. 2015). Finally, the effect of gravity load on both; the mirror
118 shape and the quality of concentrator for parabolic trough was examined by (Meiser et al.
119 2017). With the aid of finite element technique and of some specific lab tests, different
120 collector angles were studied. According to their results, the optimum collector angle, with
121 respect to the mirror shape, was 0° (zenith).

122 While, as it is presented, many configurations of receivers and absorbers have been
123 investigated in the literature, very few studies experimentally investigated and validated their
124 works are found in the literature. In this study, a lightweight solar dish concentrator which is
125 consisted of 11 curvilinear trapezoidal reflective petals, coupled with a spiral absorber inside
126 housing is manufactured and experimentally examined. This system is innovative and its
127 design has been presented in an older preliminary study done by (Pavlović et al. 2016). In this
128 study, experimental results of this collector are presented, as well as the results of a developed
129 numerical model in Engineering Equation Solver (EES) (Klein 2015) are presented. This
130 model is also used for analyzing the collector parametrically, examining various working
131 fluids. More specifically, the collector is analyzed for operation with thermal oil and water,
132 apart from water, for various temperature levels. The optimum volumetric flow rate for every
133 working fluid is determined from an energetic and exergetic sensitivity analysis. The final
134 results of this study can be used for determining the operating of this collector in medium
135 temperature levels for applications as solar cooling, electricity production, cogeneration, and
136 trigeneration.

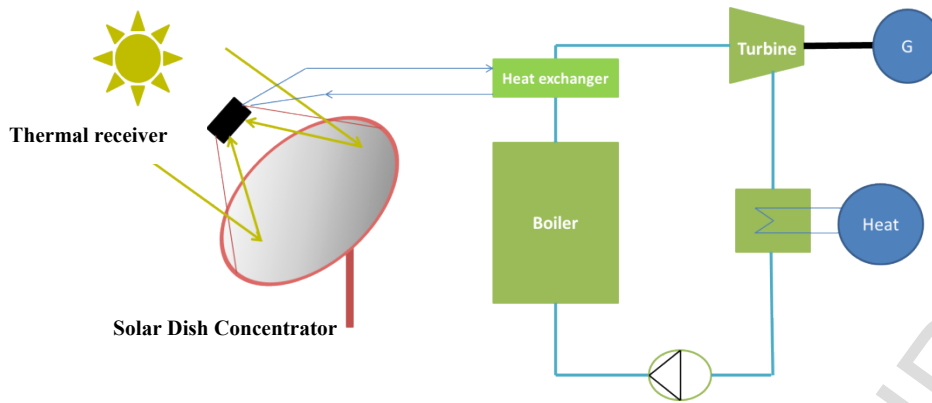
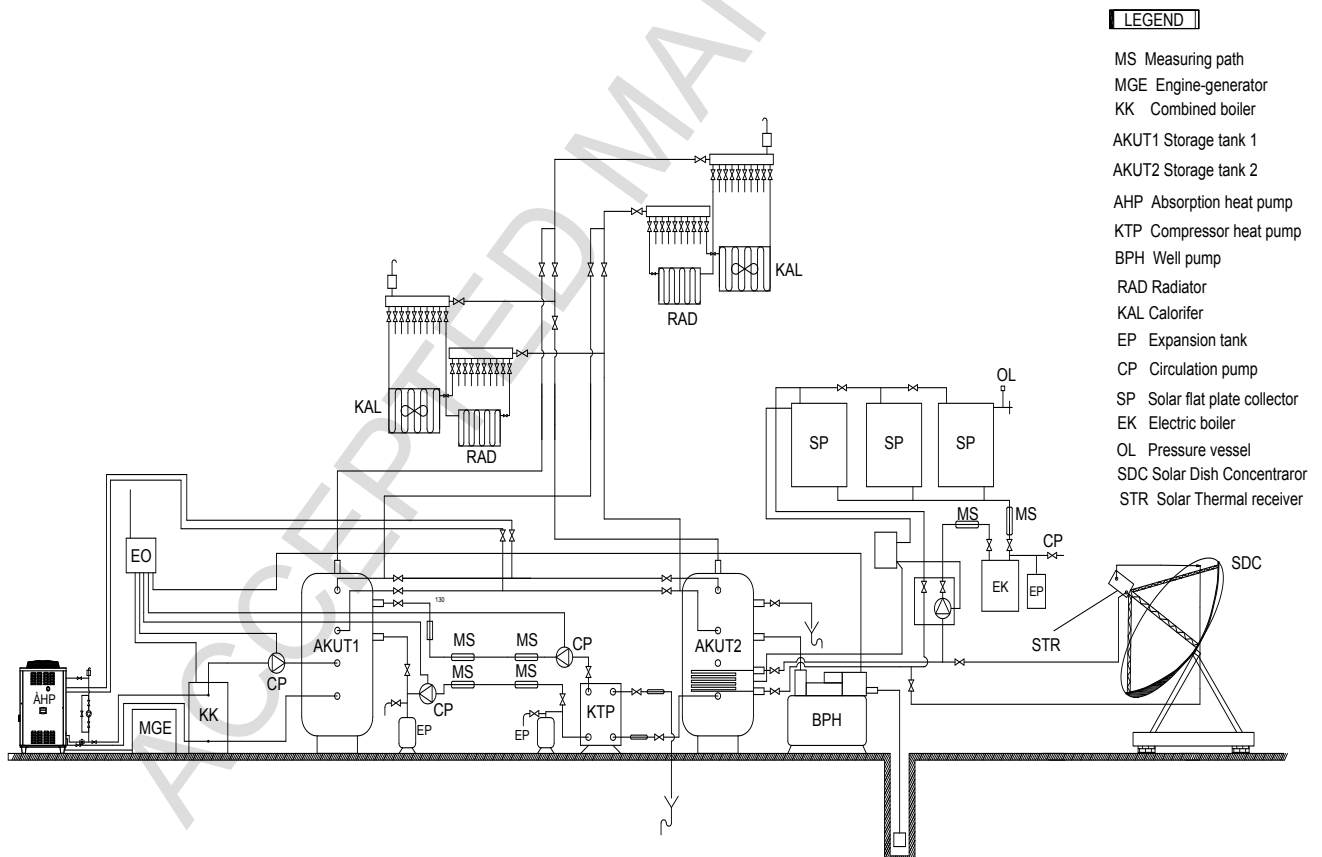


Fig. 1: Cogeneration plant with solar dish concentrating collector.

137

138 The present Fig.1 shows a cogeneration plant where solar radiation is utilized. More
 139 specifically, the solar energy is exploited with a solar dish concentrator and it is used for
 140 superheating the water in a Rankine cycle. This Rankine cycle produces electricity and
 141 simultaneously useful heat in its condenser. This hybrid system is innovative and it utilizes
 142 solar radiation for producing working fluid with high temperatures at the inlet of steam
 143 turbine.



144
 145

Fig. 2: Schematic diagram of the laboratory plant.

146 The plant in Fig.2 consists of the following polygeneration modules: solar parabolic dish
 147 concentrator, absorption heat pump, engine with generator and hot - water boiler. Heat supply
 148 during the period of reduced availability of solar power is carried out using hot water boiler.

149 Cooling effect is achieved using absorption heat pumps. The availability of solar energy use
 150 was increased by applying the accumulators' hot and cold working medium. Polygeneration is
 151 an energy system which is capable of producing several energy services using one or more
 152 sources of primary energy. Experimental hybrid polygeneration laboratory installation uses
 153 the principles of integration processes, modular structures, hybridity to provide local energy
 154 needs in terms of heating and air-conditioning systems to the production of electricity using
 155 renewable energy sources-solar energy and biomass, or alternatively by using gas or
 156 electricity. Possibility of using gas and electricity contributes to system availability and
 157 security of the local energy supply in periods of insufficient availability of renewable energy
 158 sources. The laboratory plant consists of the following modules: combined biomass boiler
 159 (KK), storage tank 1 (AKUT1), storage tank 2 (AKUT2), measurement paths (MS), electric
 160 boiler (EK), solar dish concentrator, engine-generator (MGE), compressor heat pump (KTII)
 161 and absorption heat pump (ATII), well pump (BPH).



162
 163 **Fig. 3:** Carried installation with tanks heat and cooling energy within the experimental demonstration of the
 164 laboratory system.



166
 167 **Fig.4:** The units employed for production of heat, electricity and cooling energy.

168 2. Model description

169 The examined collector is a concentrating collector with dish reflector. Fig.5 illustrates this
 170 system with the main described parts. The solar dish reflector is consisted of 11 curvilinear
 171 trapezoidal reflective petals constructed by PMMA with silvered mirror layer. The 12th part of
 172 the reflector is missing because of the existence of the bracket for supporting the system.

173 The absorber is a corrugated spiral tube which is located inside aluminum housing. The
 174 absorber is created from stainless steel and it has not selective surface. This collector has been
 175 created from low cost materials in order to reduce the total investment cost. The objective of
 176 this strategy is to create a low cost system with sufficient performance. The total cost of the
 177 system is about 7,000 €. The detail cost of each component used in the system is given as
 178 follows:

179 - Tracking system: 2,000 €

180 - Reflectors: 2,000 €

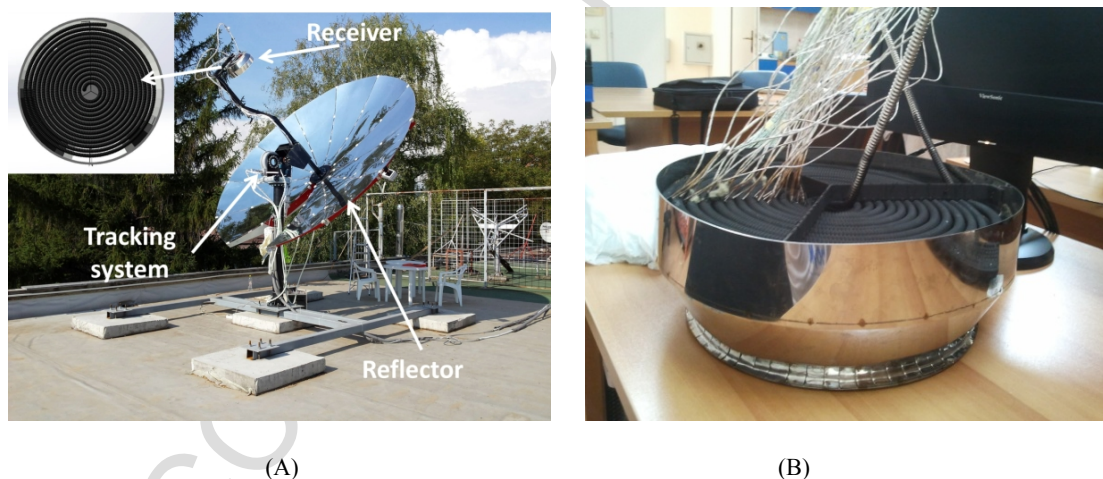
181 - Receiver with housing and support mechanism: 500 €

182 - Measuring equipment: 1,000 €

183 - Other costs: 1,500 €

184 Except from the low cost, this collector is a lightweight construction and its installation is
 185 simpler than other similar systems.

186 Table 1 includes the main data for the collector characteristics. Geometrical characteristics, as
 187 well as thermal and optical properties are given. It is interesting to state that the final
 188 reflectance is about 60%, a low value which is selected due to the dust and the stains in the
 189 mirrors. The high emittance of the absorber is a result of the low cost and consequently low
 190 quality material of the tube. The geometry of this system has been also described in a study
 191 done by (Pavlović et al. 2016) with more details.



192

(A)

(B)

193 **Fig. 5:** The examined solar parabolic concentrating system (A); and (B) solar thermal receiver.

194

195

196

197

198

Table 1. Basic parameters of the examined concentrating collector

Parameter	Value
Concentration ratio	28.26
Concentrator diameter	3.80 m
Paraboloid rim angle	45.6°
Focal distance	2.26 m
Collector aperture	10.29 m ²
Spiral length	9.5 m
Spiral outer mean diameter	12.2 mm
Spiral inner maximum diameter	11.7 mm
Spiral inner mean diameter	10.5 mm
Spiral inner minimum diameter	9.3 mm
Absorber emittance	0.9
Absorber absorbance	0.9
Mirror reflectance	0.7
Distance between absorber and reflector base	2,100 mm

199

200 3. Mathematical modelling

201 In this section, the equations which describe the developed mathematical model for simulating
 202 the thermal analysis of the collector are given. It is essential to state that this model is a
 203 simplified model which assumes uniform heat flux over the absorber.

204 3.1 Solar radiation utilization

205 The concentrated collectors with high concentrating ratios, as the examined dish reflector,
 206 utilize only the direct beam solar radiation (G_b) and the available solar energy is calculated as
 207 the product of the effective dish aperture (A_a) and the beam radiation:

$$208 \quad Q_s = A_a \cdot G_b, \quad (1)$$

209 The concentration ratio of the collector (C) is the ratio of the available aperture (A_a) to the
 210 receiver area (A_r), as Eq. (2) shows:

$$211 \quad C = \frac{A_a}{A_r}, \quad (2)$$

212 The rate of absorbed energy from the receiver (Q_{abs}) can be calculated using the optical
 213 efficiency of the collector (η_{opt}):

$$214 \quad Q_{abs} = \eta_{opt} \cdot Q_s, \quad (3)$$

215 3.2 Thermal analysis

216 The developed thermal analysis model is based on the energy balance in the receiver. The rate
 217 of absorbed solar radiation is separated to the rate of useful energy (Q_u) and to the rate of
 218 thermal losses to the environment (Q_{loss}), as Eq. (4) shows:

$$219 \quad Q_{abs} = Q_u + Q_{loss}, \quad (4)$$

220 The useful heat output can be calculated by the energy balance in the fluid volume, according
221 to Eq. (5):

$$222 \quad Q_u = m \cdot c_p \cdot (T_{out} - T_{in}), \quad (5)$$

223 The rate of thermal losses is separated to radiation (Q_{rad}) and convection (Q_{con}) losses.
224 Equations (6); (7) give the formulas for estimating these quantities:

$$225 \quad Q_{rad} = A_{ro} \cdot \varepsilon_r \cdot \sigma \cdot (T_r^4 - T_{am}^4), \quad (6)$$

$$226 \quad Q_{conv} = A_{ro} \cdot h_{air} \cdot (T_r - T_{am}), \quad (7)$$

227 The heat convection coefficient between absorber and ambient can be calculated by the
228 following Eq. (8), as proposed by (Duffie and Beckman 2013):

$$229 \quad h_{air} = 2.8 + 3 \cdot V_{air}, \quad (8)$$

230 The thermal efficiency of the collector (η_{th}) is calculated as the ratio of the useful energy
231 output to the available solar radiation:

$$232 \quad \eta_{th} = \frac{Q_u}{Q_s}, \quad (9)$$

233 3.3. Heat transfer in the flow

234 In the present section the equations related to the heat transfer inside the flow are presented.
235 The rate of useful energy that the fluid gains can be calculated as:

$$236 \quad Q_u = h \cdot A_{ri} \cdot (T_r - T_{fm}), \quad (10)$$

237 The mean fluid temperature can be calculated according to Eq. (11). This temperature has also
238 been used for the determination of the thermal properties of the working fluids.

$$239 \quad T_{fm} = \frac{T_{in} + T_{out}}{2}, \quad (11)$$

240 The heat transfer coefficient for the examined case is calculated according to Eq. (12) (Zhu et
241 al. 2017):

$$242 \quad Nu = \frac{\left(\frac{f_r}{8}\right) \cdot Re \cdot Pr}{1 + 12.8 \cdot \sqrt{\frac{f_r}{8}} \cdot (Pr^{0.68} - 1)}, \quad (12)$$

243 The friction factor (f_r) has to be determined by a complex equation because the tube is
244 corrugated in the present study. The following equation is suitable for the examined case
245 (Đorđević et al. 2016):

$$246 \quad f_r = 0.316 \cdot \text{Re}^{-0.25} + 0.41 \cdot \left(\frac{D_{ri, \min}}{D_{ri}} \right)^{0.9}, \quad (13)$$

247 It is important to state that the mean internal diameter (D_{ri}) is the diameter that is used for
 248 Reynolds definition. Equations (14), (15); (16) present the characteristic numbers of Reynolds,
 249 Prandtl and Nusselt respectively:

$$250 \quad \text{Re} = \frac{4 \cdot m}{\pi \cdot D_{ri} \cdot \mu}, \quad (14)$$

$$251 \quad \text{Pr} = \frac{\mu \cdot c_p}{k}, \quad (15)$$

$$252 \quad \text{Nu} = \frac{h \cdot D_{ri}}{k}, \quad (16)$$

253 The last important parameter for this study is the pressure drop along the tube, a parameter that
 254 is calculated by using the friction factor:

$$255 \quad \Delta P = f_r \cdot \frac{L}{D_{ri}} \cdot \left(\frac{1}{2} \cdot \rho \cdot u^2 \right), \quad (17)$$

256 The velocity of the flow (u) is calculated from the mass flow rate, according to Eq. (18):

$$257 \quad u = \frac{m}{\left(\frac{\pi}{4} \cdot D_{ri}^2 \right) \cdot \rho}, \quad (18)$$

258 3.4 Exergetic performance

259 The exergetic (or second law) evaluation of the solar collector is a useful analysis which
 260 shows the quality of the process. In the exergetic analysis, the thermal performance and the
 261 operating temperature level are taken into account, as well as the pressure drop in the tube.

262 The useful exergy output (E_u) is equal to the useful heat minus the irreversibilities of the
 263 heating process. Equation (19) shows that these irreversibilities can be expressed via the
 264 entropy generation:

$$265 \quad E_u = Q_u - T_{am} \cdot \Delta S, \quad (19)$$

266 This equation can be transformed to the following formula (Bellos et al. 2016d):

$$267 \quad E_u = Q_u - m \cdot c_p \cdot T_{am} \cdot \ln \left[\frac{T_{out}}{T_{in}} \right] - m \cdot T_{am} \frac{\Delta P}{\rho \cdot T_{fm}}, \quad (20)$$

268 The exergy of the solar radiation is calculated by the Petela model, which is the most accepted.
 269 Sun is not a heat reservoir but a radiation reservoir and for this reason there is an extra term in
 270 Eq. (21), as stated by (Bellos et al. 2016b).

$$271 \quad E_s = Q_s \cdot \left[1 - \frac{4}{3} \cdot \left(\frac{T_{am}}{T_{sun}} \right) + \frac{1}{3} \cdot \left(\frac{T_{am}}{T_{sun}} \right)^4 \right], \quad (21)$$

272 The sun temperature (T_{sun}) can be taken equal to 5770 K, a mean value in the outer surface of
 273 the sun. It is important to note that the temperature levels in Eq. 20; Eq. 21 have to be in
 274 Kelvin degrees. The exergetic performance of the solar collector is defined as the ratio of the
 275 useful exergy output to the solar exergy input, according to Eq. (22) as follows (Bellos et al.
 276 2017):

$$277 \quad \eta_{ex} = \frac{E_u}{E_s}, \quad (22)$$

278 4. Experimental design and numerical modelling

279 The first part of this study is the experimental investigation for the examined collector. For
 280 this reason the results, of a sunny day, are presented in order to evaluate both; the energetic
 281 and exergetic performance of the collector. After that, these results are compared with a
 282 developed 1-D numerical model for the sake of validation. After validating this model, the
 283 collector is investigated numerically for more operating conditions. More specifically, three
 284 working fluids (water, thermal VP-1 and air) are investigated for various flow rates and fluid
 285 inlet temperature levels. These working fluids are compared energetically and exergetically for
 286 their optimum flow rate values.

287

288 4.1 Experimental setup

289 The experimental setup has been installed in the solar lab of the Faculty of Mechanical
 290 Engineering in Nis (latitude 43°19' and longitude 21°54'). The solar dish collector is
 291 connected with a storage tank of 1,000 L. The measurement period was the last days of August
 292 and the first days of September. In the experimental setup there were many sensors in order to
 293 measure the adequate parameters. For instance, a flowmeter was used to measure the
 294 volumetric flow rate (V). Two thermometers (Pt 500) were used in order to measure the water
 295 inlet (T_{in}) and outlet temperature (T_{out}) values. Likewise, the ambient temperature (T_{am}) and
 296 the air velocity (V_{air}) were measured in a place close to the collector. The solar beam radiation
 297 is measured by using two pyranometers for the global (G) solar radiation and the diffuse (G_d)
 298 one. The time step was set to 30 s, which is considered as an adequate value for investigating
 299 this system. The main equations for the process of the experimental results are given below.
 300 Mass flow rate calculation, solar beam radiation intensity, thermal efficiency and exergetic
 301 efficiency are given in Eqs. (23), (24), (25); (26). It is important to state that in Eq. 26, the
 302 temperature values have to be in Kelvin.

$$303 \quad m(kg/s) = \frac{\rho(kg/L) \cdot V(L/h)}{3,600(s/h)}, \quad (23)$$

$$304 \quad G_b = G - G_d, \quad (24)$$

$$305 \quad \eta_{th} = \frac{m \cdot c_p \cdot (T_{out} - T_{in})}{A_a \cdot G_b}, \quad (25)$$

$$306 \quad \eta_{ex} = \frac{m \cdot c_p \cdot (T_{out} - T_{in}) - m \cdot c_p \cdot T_{am} \cdot \ln \left[\frac{T_{out}}{T_{in}} \right] - m \cdot T_{am} \frac{\Delta P}{\rho \cdot T_{fm}}}{A_a \cdot G_b \cdot \left[1 - \frac{4}{3} \cdot \left(\frac{T_{am}}{T_{sun}} \right) + \frac{1}{3} \cdot \left(\frac{T_{am}}{T_{sun}} \right)^4 \right]}, \quad (26)$$

307 Also, it is essential to mention that the intercept factor (γ) of the system was estimated to 65%,
 308 after taking into account the errors in the system design, as it is constructed at low cost. The
 309 optical efficiency is estimated by Eq. (27). This result is used in the numerical model which is
 310 described in section 4.2. More specifically, the reflectance is selected 60%, the absorbance
 311 90% and the intercept factor 65%.

$$312 \quad \eta_{opt} = (reflec\ tan\ ce) \cdot (absorbance) \cdot (int\ ercept\ factor) \approx 0.6 \cdot 0.9 \cdot 0.65 = 0.35 \quad (27)$$

313 4.2 Developed numerical model

314 The developed numerical model is a 1-D thermal model, which is based on the energy balance
 315 on the absorber. A uniform temperature level in the absorber is the key factor that has to be
 316 calculated in every case. This strategy has also been followed in (Bellos et al. 2016d) and it is
 317 a validated method for concentrating solar collectors. The calculations have been determined
 318 using (EES) which is a powerful tool for these problems. The properties of water, Therminol
 319 VP-1 and air have been taken from the EES library, (Association 1967) and (Lemmon et al.
 320 2000). Fig.6 exhibits a simple flow chart of the followed methodology for the numerical
 321 model. It is essential to note that water is studies for inlet temperature level up to 85 °C and the
 322 other working fluids up to 300 °C.

323 In the validation of the numerical model from the experimental results, a simple strategy has
 324 been followed. More specifically, many operating points have been selected and in every case,
 325 the water outlet temperature and the thermal efficiency are compared. For every examined
 326 case, the water inlet temperature, the solar beam radiation, the volumetric flow rate, the
 327 ambient temperature and the air velocity are inserted in the numerical model in order to
 328 simulate the respective real conditions of the experiment. The outlet temperature is the most
 329 important parameter because this is fully connected with the useful heat and the thermal
 330 efficiency.

331

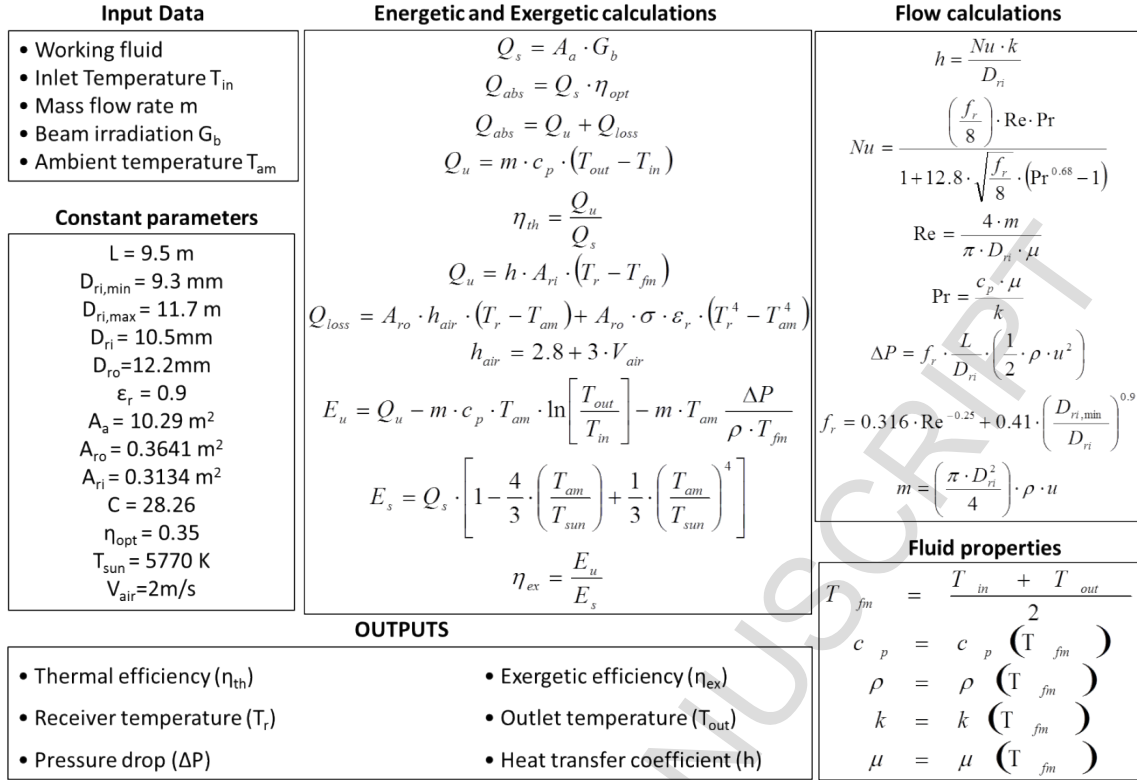


Fig. 6: Flowchart of the developed numerical model.

332

333

334 **5. Results**

335 In this section, the experimental and numerical results are presented. Section 5.1 includes the
 336 experimental results and the validation of the developed numerical model. The other two
 337 sections (5.2 and 5.3) are devoted for the working fluids investigations with the numerical
 338 model. The optimum volumetric flow rate for every case is selected according to the results of
 339 section 5.2 and the working fluid comparison is presented in section 5.3 with details.

340 **5.1 Experimental results and validation**

341 In this section both the experimental and numerical results have been presented and
 342 discussed. The collector has been examined for many days and the post representative day (3rd
 343 of September) has been selected to be presented. Energetic and exergetic results are given in
 344 the following graphs and the respective comparison with the numerical model is also
 345 presented.

346 Fig.7 shows the solar radiation during the examined day. The beam radiation is close to the
 347 total because the examined day was sunny. The solar beam radiation is the part of the total
 348 radiation that can be utilized by the collector. The exact values of the solar beam radiation are
 349 given in Table 2. In addition the ambient temperature is given in the same Table. The air
 350 velocity was about 2 m/s during the examined day.

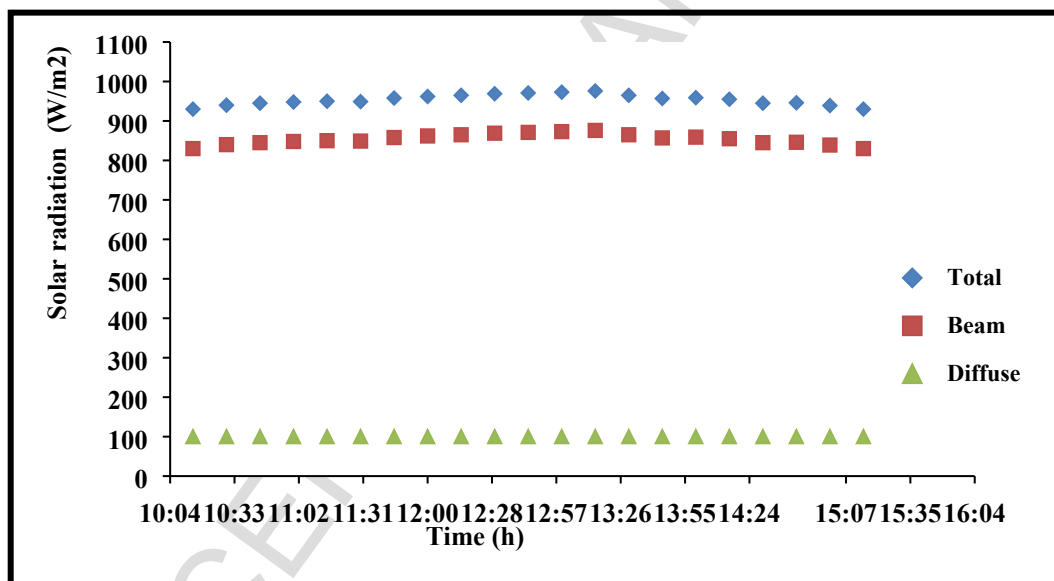
351 The most critical parameter of the experimental results is the water outlet temperature. This
 352 parameter leads to useful energy and to thermal efficiency calculation. Fig.8 depicts the
 353 comparison of the water outlet temperature from the experiments and from the numerical
 354 model. According to the results, the difference is very small, about 1.1%. Table 2 includes the

355 arithmetic results for the examined points. It is interesting to state that the outlet temperature is
 356 getting greater during the collector operation, because the inlet temperature has also an
 357 increasing rate. The storage tank aids the system to store energy and to operate in higher
 358 temperature levels during the examined day.

359 The thermal efficiency and the exergetic efficiency are depicted in Figs. 9 and 10 respectively.
 360 Table 2 also includes the values of the thermal efficiency and the comparison between the
 361 experimental and the numerical results is clear for the thermal performance. The mean thermal
 362 efficiency deviation is about 4.97%; an accepted value which validates the numerical model.
 363 According to Fig.9, the thermal performance of the collector is about 34%, a low value which
 364 is explained by the low optical performance, as it has been explained in previous sections. The
 365 exergetic performance which is given in Fig.9 is lower than 2.5% because of the low operating
 366 temperature levels of the collector.

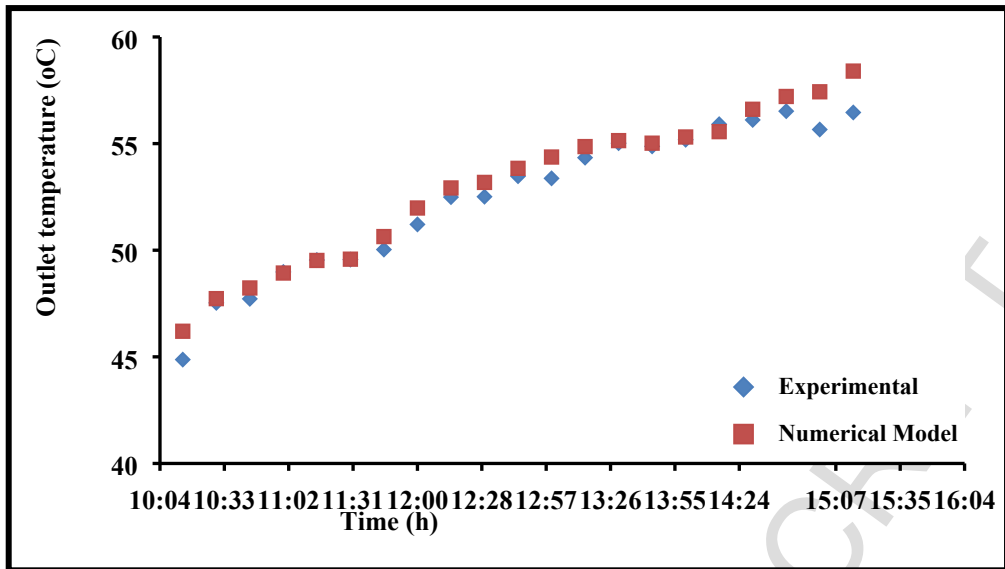
367 In the last graph of this section, Fig.11, the receiver and the mean fluid temperature levels are
 368 shown. The results are calculated numerically for all the examined cases. These temperature
 369 levels are close to each other because of the high heat convection coefficient, which is also
 370 given in the same graph. The high values of this coefficient are explained by the corrugated
 371 tube which creates turbulent flow conditions.

372



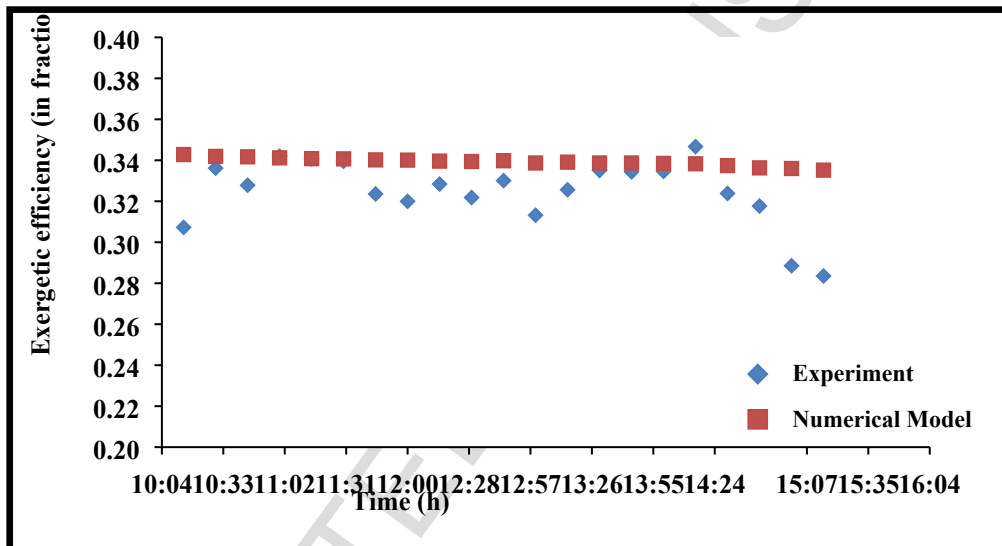
373
 374

Fig. 7: Solar radiation for the examined day.



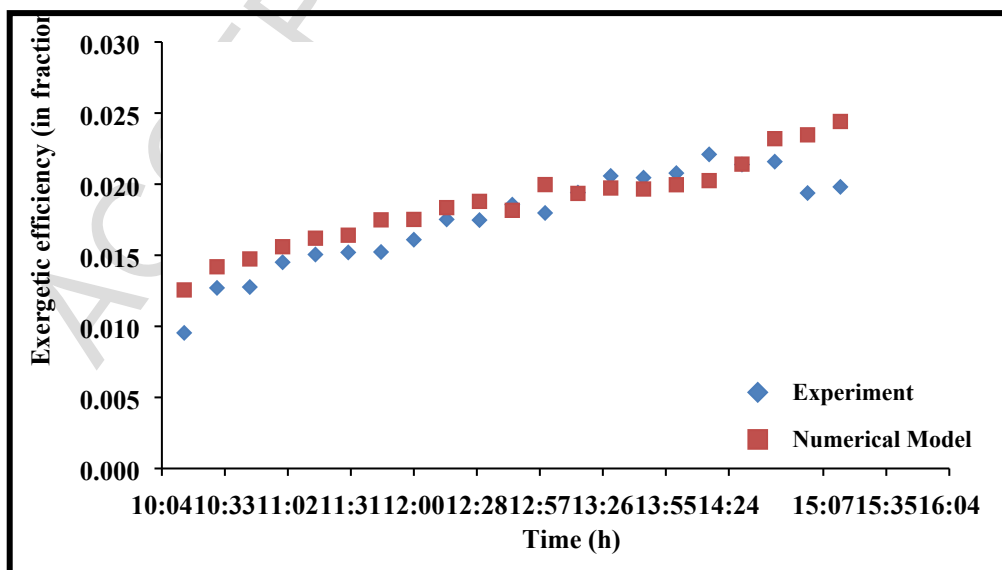
375
376

Fig. 8: Water outlet temperature level for the examined day.



377
378

Fig. 9: Thermal efficiency for the examined day.



379
380

Fig. 10: Exergetic efficiency for the examined day.

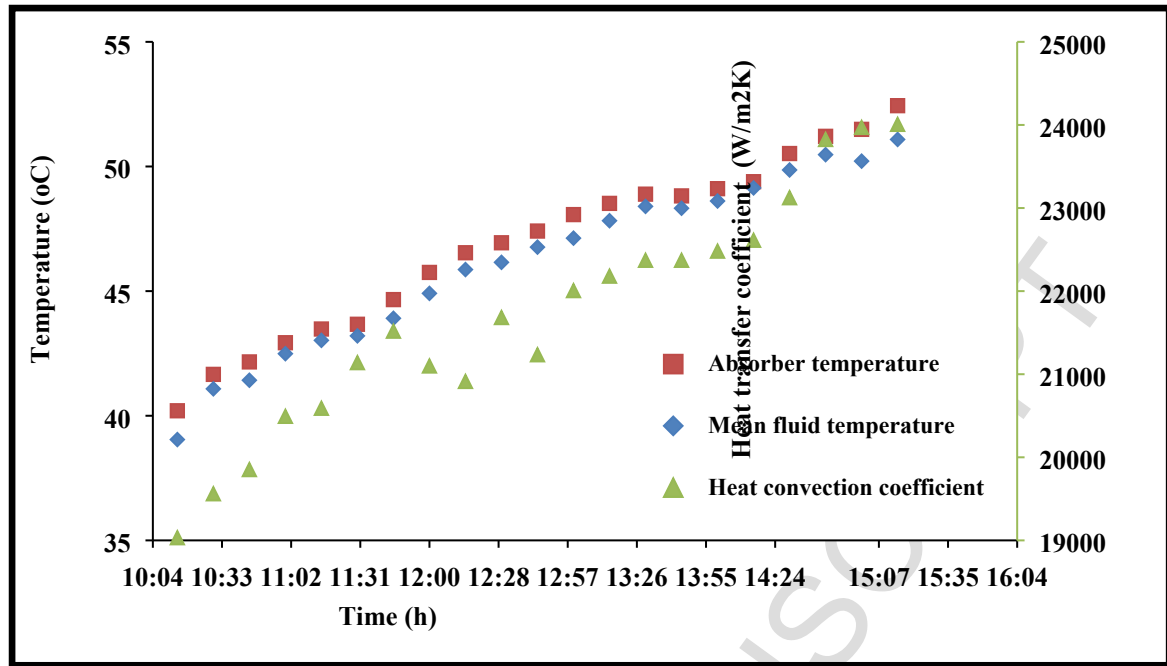


Fig. 11: Absorber temperature, fluid temperature and heat transfer coefficient calculated by the numerical model for the examined day.

381
382
383
384
385

Table.2. Comparison between the experimental and the numerical model results

Time (hr)	Measured parameters			Experimental		Numerical		Deviation	
	V (l/hr)	T _{in} (°C)	G _b (W/m ²)	T _{out} (°C)	n _{th} -	T _{out} (°C)	n _{th} -	T _{out} -	n _{th} -
10:15	194	33.22	830	44.87	0.3073	46.20	0.3428	2.96%	11.57%
10:30	194	34.63	840	47.53	0.3362	47.73	0.3419	0.42%	1.70%
10:45	195	35.13	845	47.72	0.3278	48.23	0.3417	1.07%	4.23%
11:00	198	36.00	848	48.98	0.3420	48.93	0.3412	0.10%	0.23%
11:15	197	36.51	850	49.54	0.3408	49.52	0.3408	0.04%	0.01%
11:30	201	36.85	849	49.56	0.3395	49.58	0.3407	0.04%	0.34%
11:45	201	37.79	858	50.03	0.3236	50.64	0.3402	1.22%	5.14%
12:00	194	38.61	862	51.21	0.3200	51.98	0.3401	1.50%	6.29%
12:15	190	39.24	865	52.49	0.3284	52.92	0.3396	0.82%	3.41%
12:30	195	39.80	869	52.51	0.3218	53.18	0.3394	1.28%	5.46%
12:45	190	40.06	871	53.47	0.3301	53.84	0.3398	0.69%	2.94%
13:00	194	40.88	873	53.37	0.3132	54.37	0.3387	1.87%	8.15%
13:15	194	41.31	876	54.34	0.3256	54.86	0.3391	0.96%	4.14%
13:30	194	41.78	865	55.02	0.3351	55.14	0.3387	0.22%	1.08%
13:45	194	41.78	857	54.87	0.3344	55.02	0.3387	0.27%	1.30%
14:00	194	42.05	859	55.18	0.3346	55.31	0.3385	0.24%	1.16%
14:15	194	42.37	855	55.91	0.3467	55.56	0.3383	0.63%	2.41%
14:30	194	43.61	845	56.11	0.3238	56.61	0.3374	0.89%	4.19%
14:45	197	44.43	846	56.52	0.3177	57.21	0.3363	1.22%	5.86%
15:00	197	44.77	839	55.66	0.2885	57.43	0.3360	3.18%	16.45%
15:15	194	45.71	830	56.46	0.2835	58.40	0.3352	3.44%	18.23%

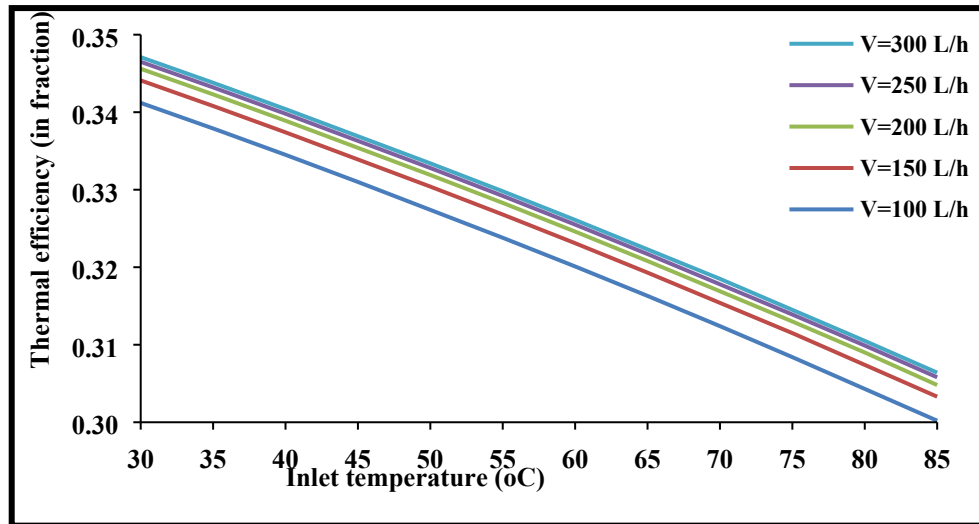
386 5.2 Working fluid investigation

387 The validated numerical model was used for further investigation of the solar
388 collector. Three working fluids are tested for various volumetric flow rates in order to estimate
389 their performance. In this section, the optimum flow rate for each working fluid is determined
390 by examining the thermal and the exergetic performance of the collector in all the operating
391 temperature range.

392 Figs. 12 and 13 illustrate the thermal and the exergetic performance of the collector for
393 operation with water. In order to keep the water in its liquid phase, the maximum temperature
394 level in the inlet was selected at 85 °C. Fig.12 shows that higher flow rate leads to higher
395 thermal efficiency. Flow rates above 150 L/h are accepted energetically, while the case of 100
396 L/h is not satisfying. Fig.13 gives the respective results exergetically, where the lower mass
397 flow rate gives higher exergetic performance. By combining these two cases, the optimum
398 flow rate is one intermediate case where thermal and exergetic performances are satisfying.
399 Thus, 200 L/h are selected to be the most appropriate solution for the water case. It is
400 interesting to note that the experimental flow rate was selected close to this value, fact that
401 proves that the experimental investigation of the collector has been performed with the
402 optimum volumetric flow rate.

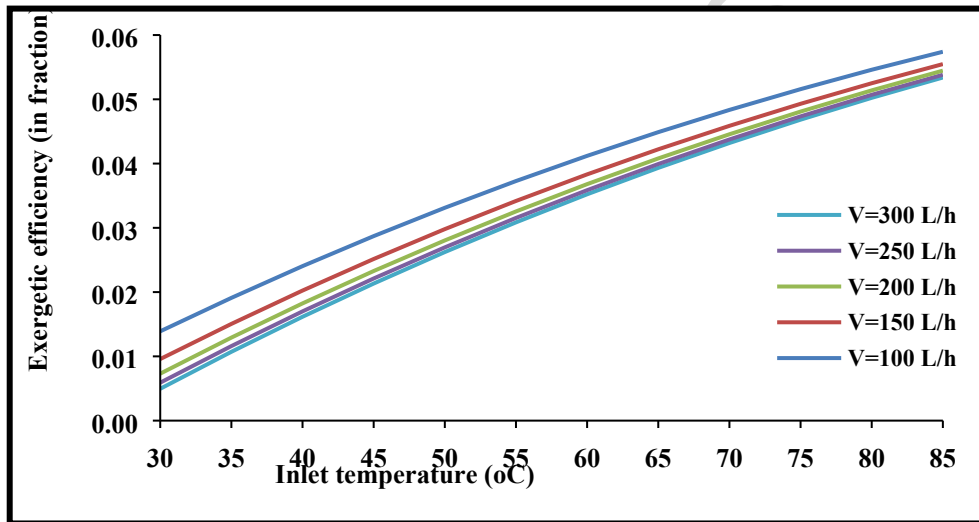
403 Figs.14 and 15 exhibit the thermal and exergetic performance for operation with Therminol
404 VP-1. Fig.10 shows that the thermal performance is enhanced with higher flow rates, with
405 values greater of 150 L/h to be accepted. The exergetic performance is very interesting
406 because of the existence of optimum operating temperature levels. The maximum performance
407 is observed, for all the mass flow rates, when the oil inlet temperature is close to 150 °C. For
408 low temperature, the lowest flow rate is the optimum, while for higher than the optimum
409 temperature; 200 L/h is the best choice. Taking into account both Figs.10 and 11; the optimum
410 flow rate again is 200 L/h.

411 Figs. 16, 17 and 18 depict the results for operating with air as working fluid. Fig.12 proves
412 that the performance of the collector is fully depended on the flow rate and values lower than
413 20 L/h are not accepted. The exergetic performance, which is given in Fig.13, proves that the
414 optimum flow rate is 25 L/h; a value which also leads to satisfying thermal performance and
415 so it is selected as the most appropriate selection. It is important to state that the examined
416 flow rates are lower than in the cases of water and thermal oil. Greater flow rates will lead to
417 extremely high pressure losses in the collector and the exergetic performance will be very low
418 or negative. Pressure drop is given in Fig.14 for the examined flow rates. According this
419 graph, greater flow rate increases the pressure drop with a high rate, a result which supports
420 the previous comment.



421
422

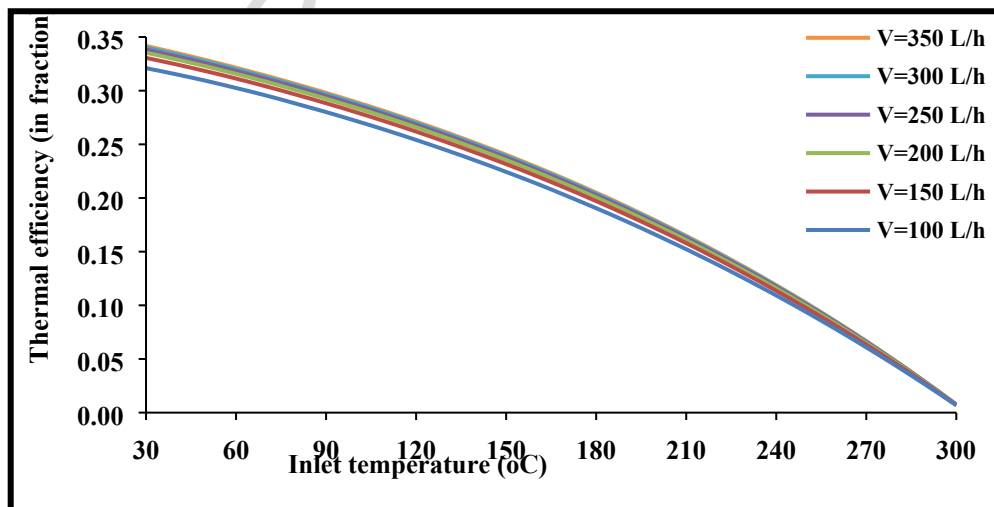
Fig. 12: Thermal efficiency for operation with water and various flow rates.



423
424

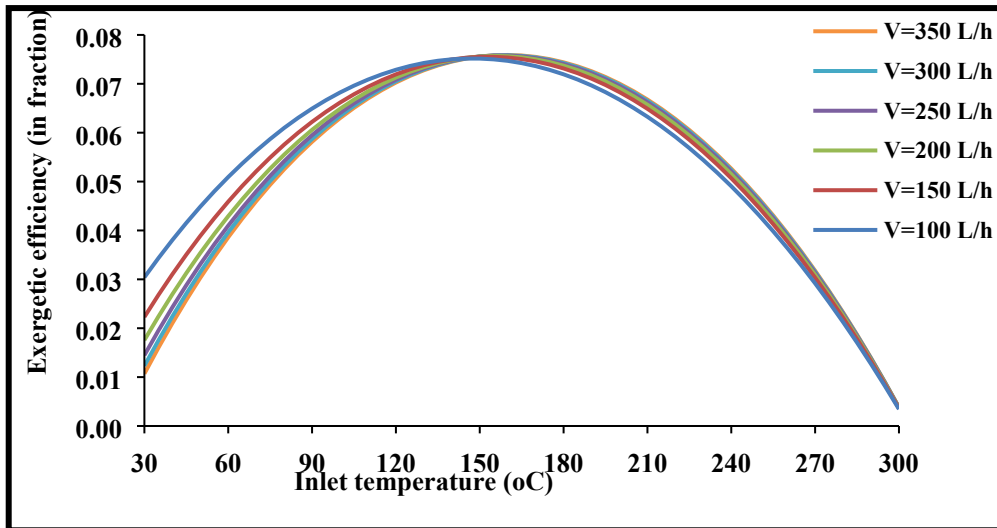
Fig. 13: Exergetic efficiency for operation with water and various flow rates.

425



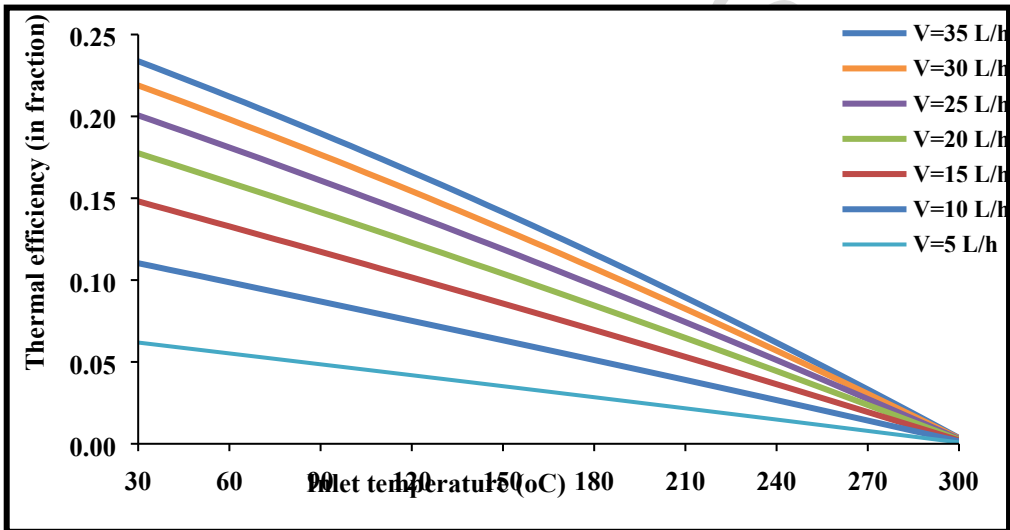
426
427

Fig. 14: Thermal efficiency for operation with Therminol VP-1 and various flow rates.



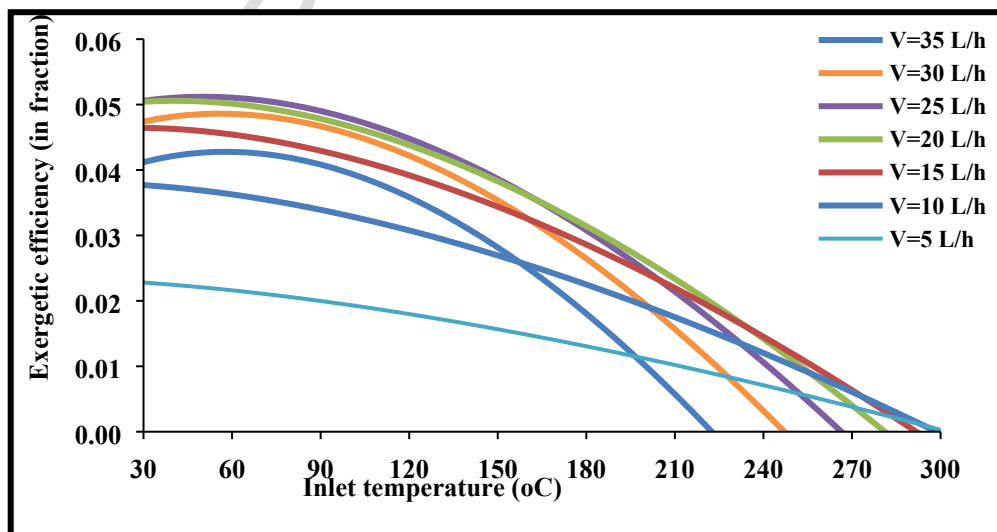
428
429

Fig. 15: Exergetic efficiency for operation with Therminol VP-1 and various flow rates.



430
431
432

Fig. 16: Thermal efficiency for operation with air and various flow rates.



433
434

Fig. 17: Exergetic efficiency for operation with air and various flow rates.

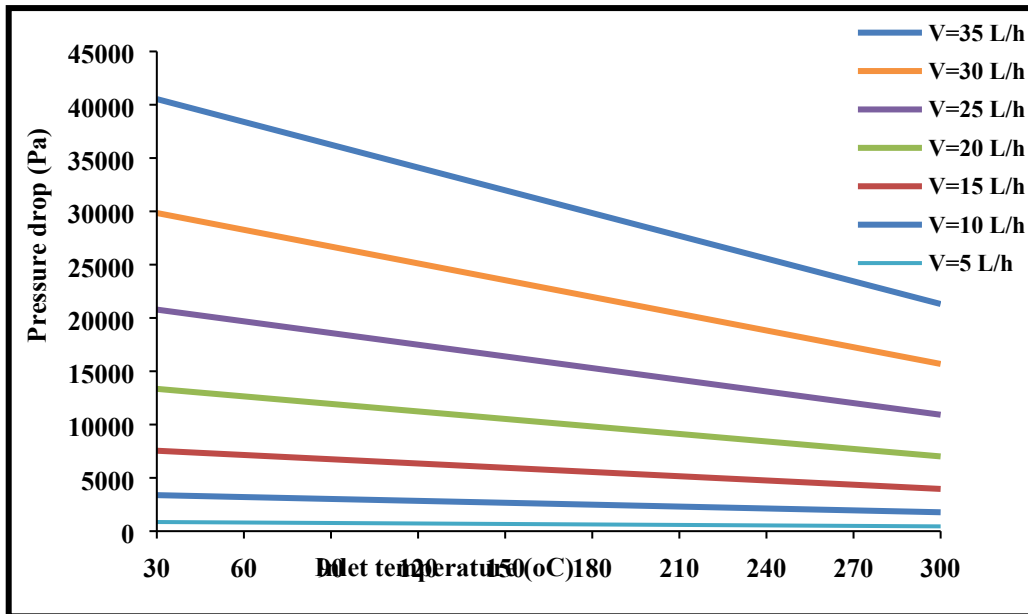


Fig. 18: Pressure drop for operation with air and various flow rates.

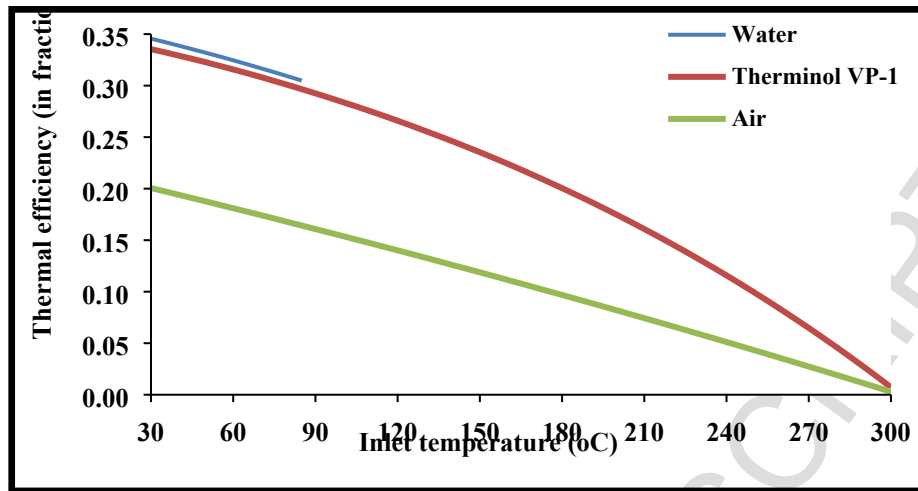
435
436

437 5.3 Comparison of the working fluids

438 In this section the comparison of the examined working fluids is presented. For every
 439 working fluid, its optimum volumetric flow rate has been selected in order to perform a
 440 suitable comparison. Fig.19 shows the thermal comparison among the working fluids. Water is
 441 the best choice for lower temperature levels, while thermal oil is better for higher temperature
 442 levels. Air is not the best choice in any temperature level. Fig.20 illustrates the exergetic
 443 efficiency for all the working fluids. For low temperature levels, air seems to be the better
 444 fluid exergetically while for greater temperature levels; Therminol VP-1 performs better. The
 445 maximum exergetic performance is achieved for operation at 155 °C and it is 7.57%. The
 446 reason for the high exergetic performance of the air in low temperature levels is the low flow
 447 rate which is conjugated with high temperature increase. This result aid the system to have
 448 high exergetic performance. However, in higher temperature levels, the low thermal efficiency
 449 of the air case makes the exergetic performance to be reduced with a high rate, making thermal
 450 oil case the optimum. The outlet temperature levels for all the examined cases are given in
 451 Fig.21. It is interesting that the air case curve has a small slope, compared to the other curves.
 452 This result comes in accordance with the previous comments about the exergetic performance.
 453 The receiver performance is given in Fig.22 and the results are similar to Fig.18. Higher
 454 receiver temperature leads to higher rate of thermal losses and to lower thermal performance.
 455 It is noticeable that this observation is validated by the results of Fig.15. What is more, by
 456 studying Figs. 15 and 18 together, the stagnation temperature of the collector can be estimated
 457 to 300 °C, because in this receiver temperature level the thermal efficiency is practically zero.
 458 The receiver temperature is fully connected with the heat transfer coefficient which is given in
 459 Fig.23. For the water case, this parameter takes high values, something that explains the higher
 460 thermal performance of the water, according to Fig.15.

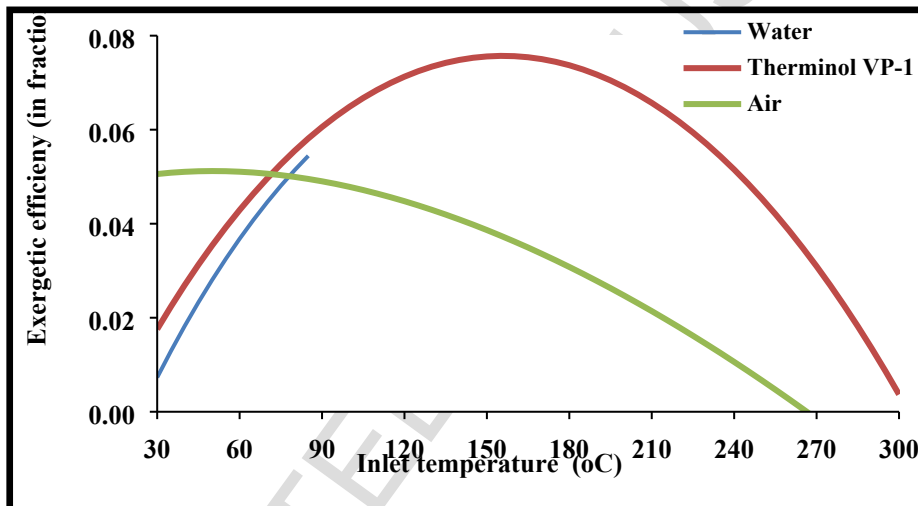
461 The last presented parameter in this working fluid comparison, is the pressure drop. This
 462 parameter takes extremely high values for the case of air, a result that have been also noticed
 463 in the previous section. Thermal oil and water present similar pressure losses because these
 464 fluids are liquids. The results of this figure indicate that the pressure loss is a significant factor
 465 for evaluating the collector in the cases of gas working fluids. The exergetic analysis takes into

466 account the pressure losses and it is the most appropriate index for evaluating the solar
 467 collector performance.



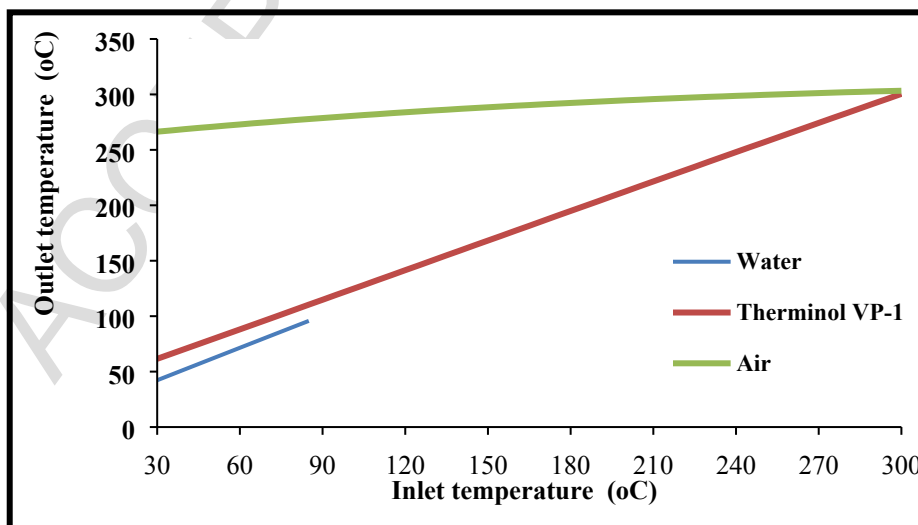
468
 469

Fig. 19: Thermal efficiency comparison among the examined working fluids.



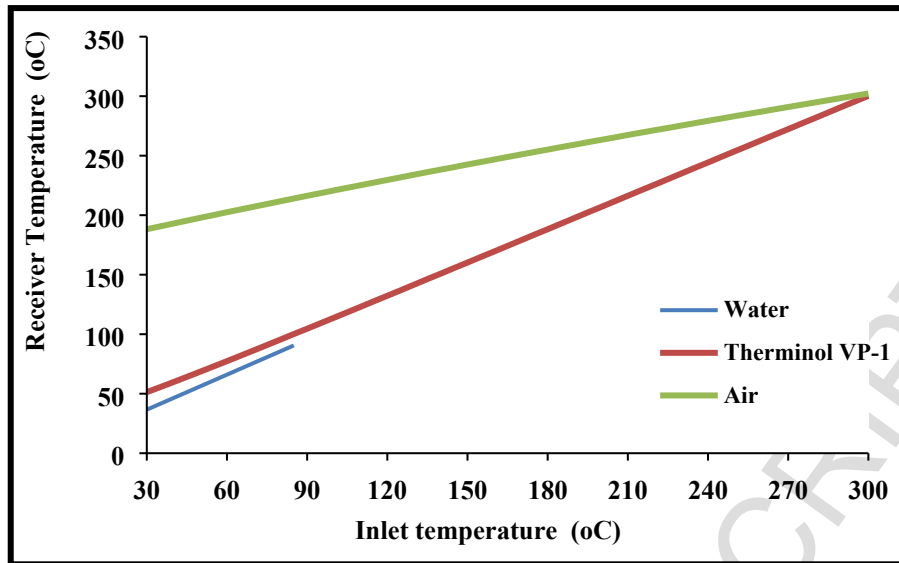
470
 471

Fig. 20: Exergetic efficiency comparison among the examined working fluids.



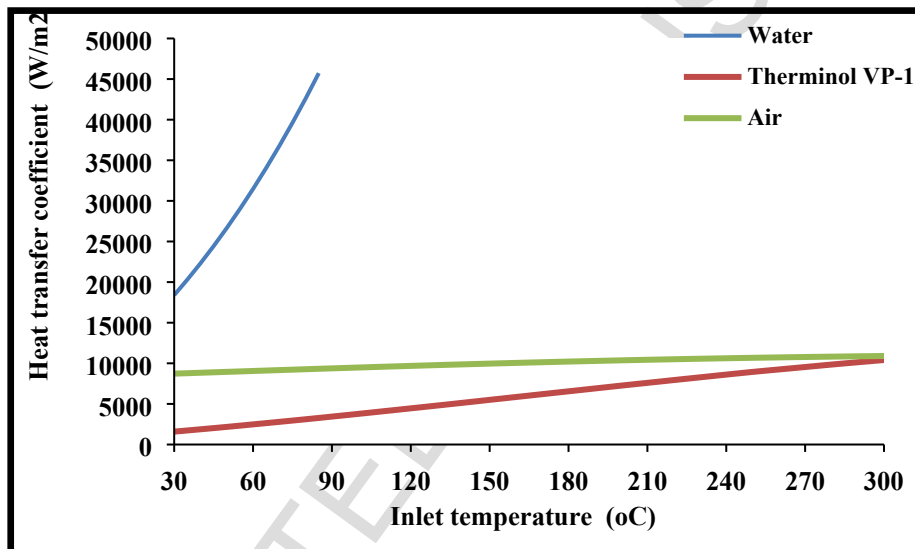
472
 473

Fig. 21: Outlet temperature comparison among the examined working fluids.



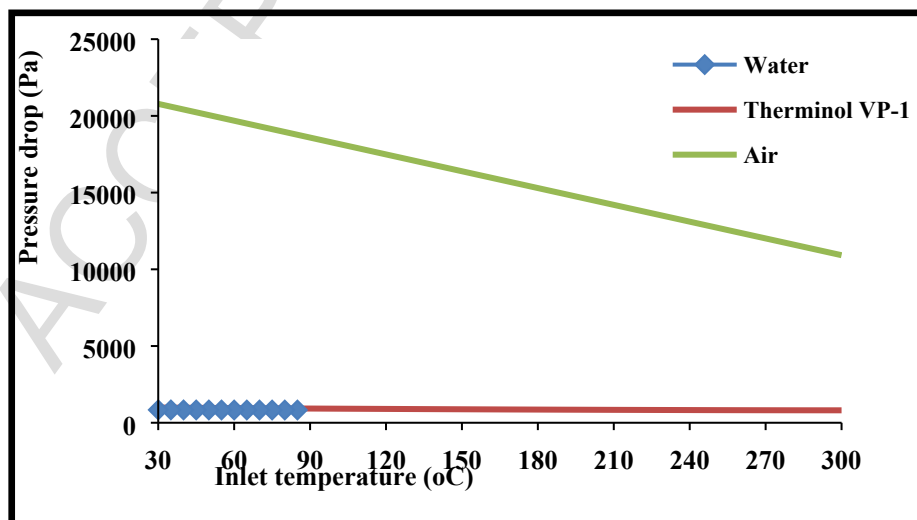
474
475

Fig. 22: Receiver temperature comparison among the examined working fluids.



476
477
478

Fig. 23: Heat transfer coefficient comparison among the examined working fluids.

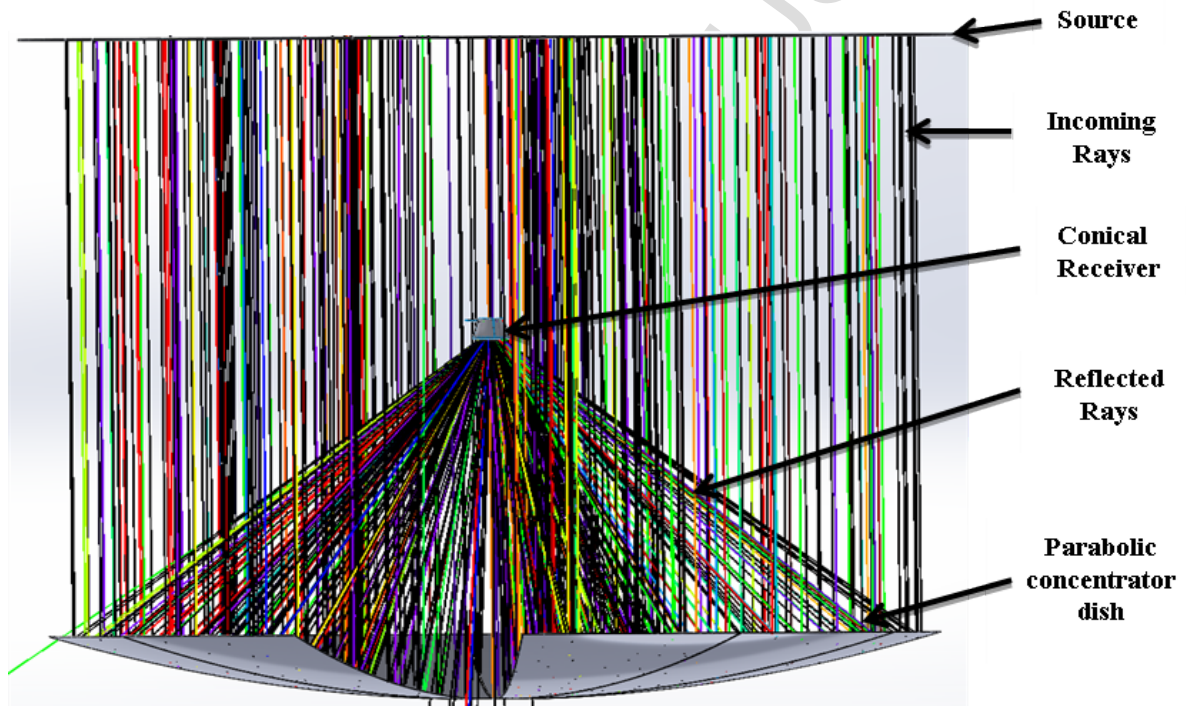


479
480

Fig. 24: Pressure drop comparison among the examined working fluids.

481 **6. Conical cavity receiver**

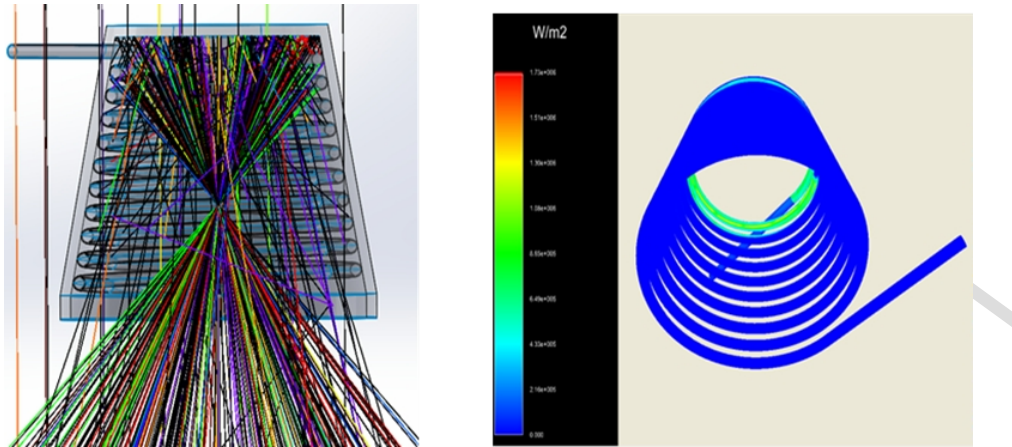
482 In this part, the optical analysis of the helical conical cavity receiver configuration, based on
 483 studies done by (Daabo et al. 2016c), has been investigated with the aim of enhancing its
 484 performance in order to enhance the overall function of the system. So, Fig.25 shows the
 485 OptisWorks analysis for the conical shape receiver where the source was set to act as sun and
 486 the same concentrator, which was presented Fig.5, was modelled in order to reflect the
 487 incoming rays to the aperture area of the conical receiver. The effect of changing the focal
 488 distance on the both; the amount of absorbed rays and their distribution on the internal surface,
 489 helical tube, of the cone can be seen in Figs.26 a, 26 b and 22 c. In Fig.26 a, when the focal
 490 distance is 2212 mm, the focal point located inside the cavity receiver, it can be noticed that
 491 the flux distributed in a bad manner on the helical tube surface where most of the rays were
 492 concentrated on the bottom of the tube, besides, the average absorbed flux was relatively low.
 493 However, the distribution was gradually enhanced by increase the focal distance, to let the
 494 focal point located outside the aperture. Specifically speaking the best distribution was
 495 achieved at 2310 mm and at the same time the average value of absorbed irradiance was also
 496 high.



497

498

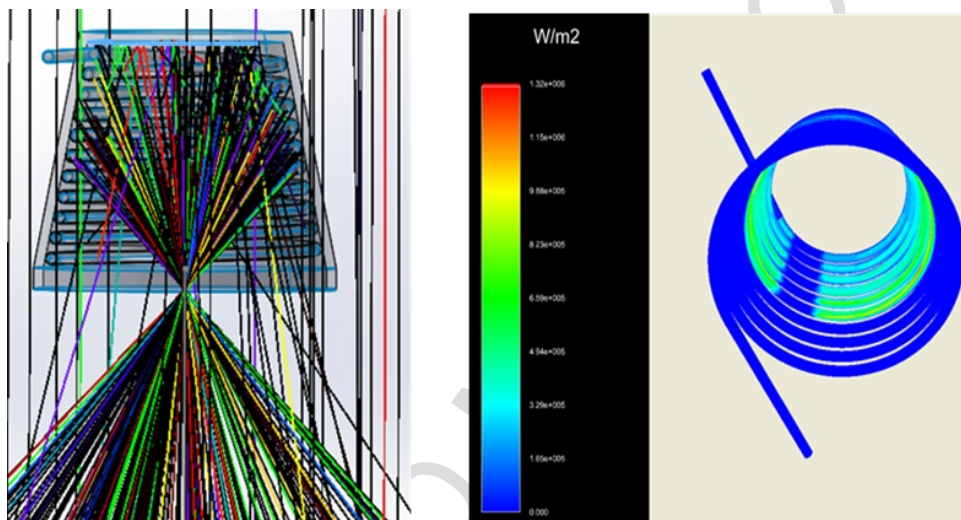
Fig. 25: Ray tracing simulation using OptisWorks 2012.



499

500

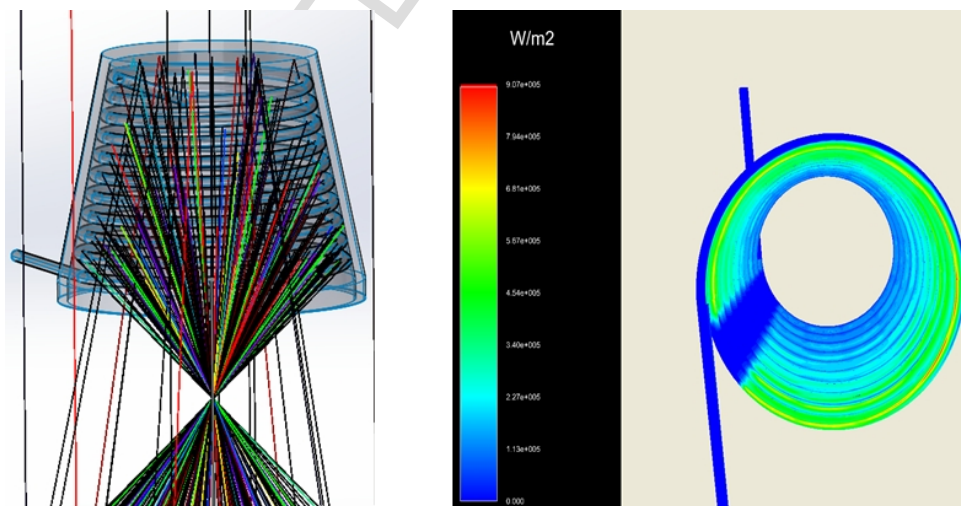
(a)



501

502

(b)



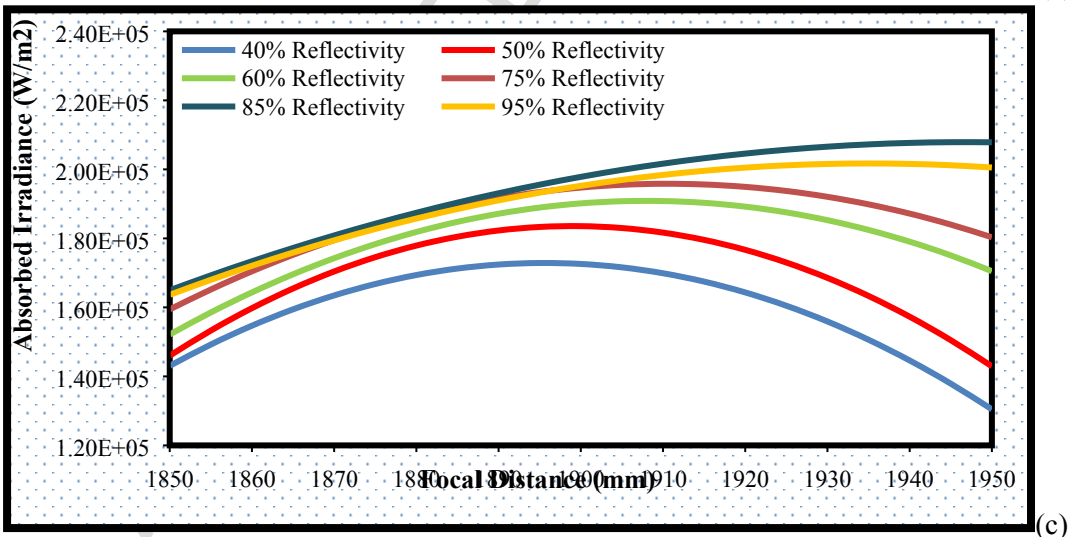
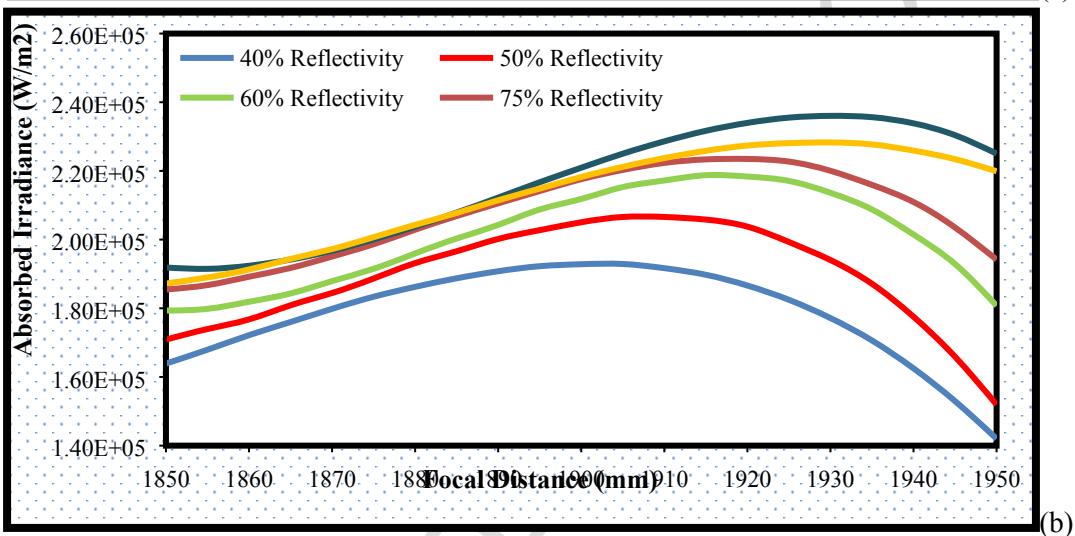
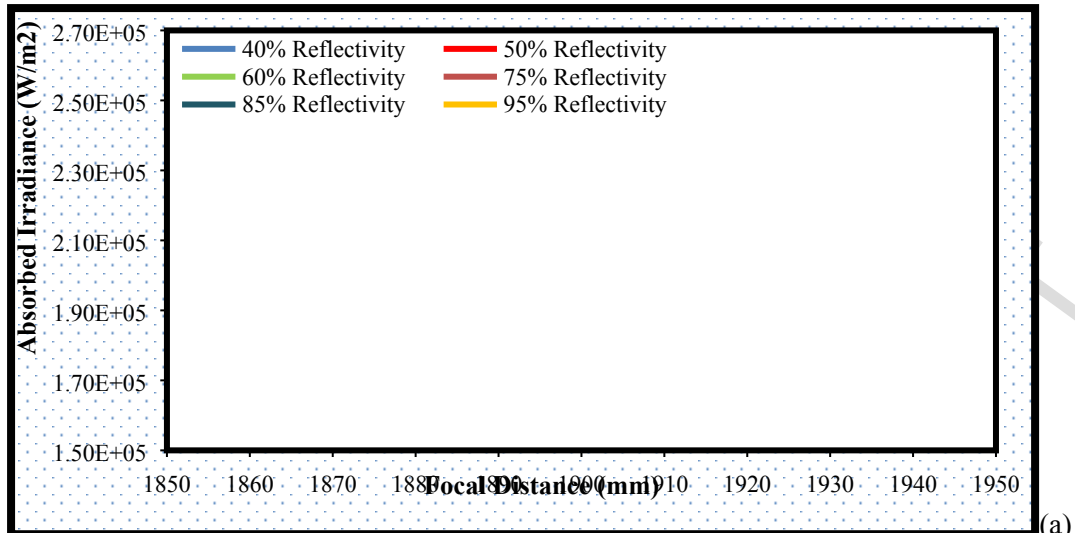
503

504

(c)

505 **Fig. 26:** The rays and flux distribution on the conical helical tube of the receiver at: (a): the focal point inside the
 506 cavity, (b): the focal point at the aperture and (c): the focal point outside the cavity.

507 The effect of focal distance values on the averaged absorbed irradiance at different
508 values of cavity surface's reflectivity is presented in Fig.27. Generally speaking, both; the
509 focal distance and the cavity reflectivity played important roles in terms of the amount of
510 absorbed flux at the three investigated absorptivity values of the tube, 100%, 95% and 85% for
511 the three graphs 27 a, 27 b and 27 c respectively. Fig.27 a, shows the mentioned effect when
512 the tube absorptivity was assumed to 100%, black body. In this figure it can be seen that the
513 average absorbed irradiance started with relatively low values, ranged between 1.75 and
514 2.0×10^5 W/m² (depending on the value of reflectivity), at focal distance of 2240 mm and
515 reached the maximum average values, which were ranged from 1.9 to 2.5×10^5 W/m² at a
516 distance of 2325 mm. Then it decreased again when the distance increased and the main
517 reason for that is the high ratio of the lost rays which were located outside the cavity receiver.
518 Similarly, Figs. 27 b and 27 c show that the highest values of absorbed irradiance were
519 achieved by shifting the conical receiver to a higher focal distance and let the concentrated
520 rays meet outside the aperture area. Having said that, the values of absorbed irradiance were
521 lower in both, 27 b and 27 c compared to 27 a, because the absorptivity values for the helical
522 tube inside the cavity receiver were assumed lower. It can be seen that the maximum values of
523 the average absorbed irradiance were ranged from 1.86 to about 2.34×10^5 W/m², and
524 between 1.65 and 2.05×10^5 W/m², at 2331 and 2337 mm for 27 b and 27 c respectively.
525 These results prove that the optimum distance between receiver and concentrator is depended
526 on the optical properties of the system.



530 **Fig. 27:** The effect of focal distance values on the averaged absorbed irradiance at different values of reflectivity for
 531 the cavity surface. When the absorptivity of the tube is 100%, (a), (b) when it is 95% and (c) when it is 85%.

532

533

534 7. Conclusions

535 A solar dish collector with a spiral coil receiver, using three working fluids (Water,
536 Therminol VP-1 and Air), has been analyzed experimentally and numerically at various
537 operating conditions. Furthermore, a numerical model was used for estimating the energetic
538 and exergetic performance of the collector in various operating cases. The main outcomes of
539 this study can be summarized as follows:

540 1- The experimental results showed that the thermal efficiency of the collector is only about
541 34%. This low performance can be justified by the low optical efficiency of the collector.

542 2- Water is the most appropriate working fluid in low temperature levels because of the high
543 heat transfer coefficient between the tube and the fluid.

544 3- The exergetic analysis proved that air seems to be a promising working fluid in low
545 temperature levels because of its high outlet temperature. The optimum flow rate is
546 significantly lower than the other two working fluids because of the impact of the pressure
547 losses on the exergetic performance.

548 4- The optimum exergetic performance was observed for the case of Therminol VP-1, as
549 working fluid, and for an inlet temperature level equal to 155 °C.

550 5- The optical analysis results showed the best location for the receiver at different optical
551 properties of the receiver's surfaces. Moreover, the conical configuration has the potential to
552 offer, by far, a higher performance than the first shape. This potential initiates an opportunity
553 for thermal analysis which will be undertaken in our next research.

554

555 Acknowledgments

556 This paper is done within the research framework of research project: III42006 – Research and
557 development of energy and environmentally highly effective polygeneration systems based on
558 renewable energy resources. Project is financed by Ministry of Education, Science and
559 Technological Development of Republic of Serbia. The experiments were conducted at the
560 Faculty of Mechanical Engineering in Nis, Laboratory for Thermal and Process Engineering.
561 A special thanks to the Higher Committee of Developing Education in Iraq HCED and the
562 University of Birmingham.

563 Nomenclature

564	A	Area, m ²
565	C	Concentration ratio, -
566	cp	Specific heat capacity under constant pressure, kJ/kg K
567	D	Diameter, m
568	E	Exergy flow, W
569	f _f	Friction factor, -
570	G	Global solar radiation, W/m ²
571	G _b	Solar beam radiation, W/m ²
572	G _d	Solar diffuse radiation, W/m ²
573	h	Convection coefficient, W/m ² K
574	k	Thermal conductivity, W/mK

575	L	Tube length, m
576	m	Mass flow rate, kg/s
577	Nu	Mean Nusselt number, -
578	Pr	Prandtl number, -
579	Q	Heat flux, W
580	Re	Reynolds number, -
581	T	Temperature, °C
582	u	Working fluid velocity, m/s
583	V	Volumetric flow rate, m ³ /s
584	V _{air}	Ambient air velocity, m/s

585 **Greek symbols**

586	γ	Heat capacity ratio, -
587	ΔP	Pressure drop, kPa
588	ΔS	Entropy increase, J/K
589	ε	Emittance, -
590	η	Efficiency, -
591	μ	Dynamic viscosity, Pa s
592	ρ	Density, kg/m ³
593	σ	Stefan–Boltzmann constant [= 5.67 · 10 ⁻⁸ W/m ² K ⁴]

594 **Subscripts and superscripts**

595	a	Aperture
596	abs	Absorbed
597	air	Ambient air
598	am	Ambient
599	ex	Exergetic
600	fm	Mean fluid
601	in	Inlet
602	opt	Optical
603	r	receiver
604	ri	Inner receiver
605	ri,max	Inner receiver max
606	ri,min	Inner receiver min
607	ro	Outer receiver
608	s	Solar
609	th	Thermal
610	u	Useful

611 **Abbreviations**

612	DNI	Direct Normal Irradiance
613	EES	Engineer Equator Solver

614 **References**

- 615 Abid, M., Ratlamwala, T. and Atikol, U. 2015. "Performance assessment of parabolic dish
616 and parabolic trough solar thermal power plant using nanofluids and molten salts."
617 International Journal of Energy Research.
618 Association, E. R. 1967. "Steam Tables, Thermodynamic Properties of Water and Steam;
619 Viscosity of Water and Steam, Thermal Conductivity of Water and Steam". City:
620 Edward Arnold Publishers, London.

- 621 Bellos, E., Korres, D., Tzivanidis, C. and Antonopoulos, K. 2016a. "Design, simulation and
622 optimization of a compound parabolic collector." *Sustainable Energy Technologies*
623 *and Assessments*, 16, 53-63.
- 624 Bellos, E., Tzivanidis, C., Antonopoulos, K. and Gkinis, G. 2016b. "Thermal enhancement of
625 solar parabolic trough collectors by using nanofluids and converging-diverging
626 absorber tube." *Renewable Energy*, 94, 213-222.
- 627 Bellos, E., Tzivanidis, C., and Antonopoulos, K. A. 2016c. "Exergetic, energetic and financial
628 evaluation of a solar driven absorption cooling system with various collector types."
629 *Applied Thermal Engineering*, 102, 749-759.
- 630 Bellos, E., Tzivanidis, C., Antonopoulos, K. A. and Daniil, I. 2016d. "The use of gas working
631 fluids in parabolic trough collectors—An energetic and exergetic analysis." *Applied*
632 *Thermal Engineering*, 109, 1-14.
- 633 Bellos, E., Tzivanidis, C., Daniil, I. and Antonopoulos, K. A. 2017. "The impact of internal
634 longitudinal fins in parabolic trough collectors operating with gases." *Energy*
635 *Conversion and Management*, 135, 35-54.
- 636 Cohen, S. and Grossman, G. 2016. "Development of a solar collector with a stationary
637 spherical reflector/tracking absorber for industrial process heat." *Solar Energy*, 128,
638 31-40.
- 639 Cui, F., He, Y., Cheng, Z. and Li, Y. 2013. "Study on combined heat loss of a dish receiver
640 with quartz glass cover." *Applied energy*, 112, 690-696.
- 641 Daabo, A. M., Al Jubori, A., Mahmoud, S. and Al-Dadah, R. K. 2016a. "Parametric study of
642 efficient small-scale axial and radial turbines for solar powered Brayton cycle
643 application." *Energy Conversion and Management*, 128, 343-360.
- 644 Daabo, A. M., Al Jubori, A., Mahmoud, S. and Al-Dadah, R. K. 2017. "Development of
645 three-dimensional optimization of a small-scale radial turbine for solar powered
646 Brayton cycle application." *Applied Thermal Engineering*, 111, 718-733.
- 647 Daabo, A. M., Mahmoud, S., and Al-Dadah, R. K. 2016b. "The effect of receiver geometry on
648 the optical performance of a small-scale solar cavity receiver for parabolic dish
649 applications." *Energy*, 114, 513-525.
- 650 Daabo, A. M., Mahmoud, S. and Al-Dadah, R. K. 2016c. "The optical efficiency of three
651 different geometries of a small scale cavity receiver for concentrated solar
652 applications." *Applied Energy*, 179, 1081-1096.
- 653 Đorđević, M., Stefanović, V. and Mančić, M. 2016. "Pressure drop and stability of flow in
654 Archimedean spiral tube with transverse corrugations." *Thermal Science*, 20(2), 579-
655 591.
- 656 Duffie, J. A. and Beckman, W. A. 2013. *Solar engineering of thermal processes*: John Wiley
657 & Sons.
- 658 Iodice, P., d'Accadia, M. D., Abagnale, C. and Cardone, M. 2016. "Energy, economic and
659 environmental performance appraisal of a trigeneration power plant for a new district:
660 Advantages of using a renewable fuel." *Applied Thermal Engineering*, 95, 330-338.
- 661 Kalogirou, S. A. 2004. "Solar thermal collectors and applications." *Progress in energy and*
662 *combustion science*, 30(3), 231-295.
- 663 Klein, S. 2015. "Engineering equation solver (EES), academic professional version, F-Chart
664 software."
- 665 Lemmon, E. W., Jacobsen, R. T., Penoncello, S. G. and Friend, D. G. 2000. "Thermodynamic
666 properties of air and mixtures of nitrogen, argon, and oxygen from 60 to 2000 K at
667 pressures to 2000 MPa." *Journal of physical and chemical reference data*, 29(3), 331-
668 385.
- 669 Li, Z., Tang, D., Du, J. and Li, T. 2011. "Study on the radiation flux and temperature
670 distributions of the concentrator–receiver system in a solar dish/Stirling power
671 facility." *Applied Thermal Engineering*, 31(10), 1780-1789.
- 672 Loni, R., Kasaeian, A., Asli-Ardeh, E. A. and Ghobadian, B. (016. "Optimizing the efficiency
673 of a solar receiver with tubular cylindrical cavity for a solar-powered organic Rankine
674 cycle." *Energy*, 112, 1259-1272.

- 675 Lovegrove, K., Burgess, G. and Pye, J. 2011. "A new 500 m² paraboloidal dish solar
676 concentrator." *Solar Energy*, 85(4), 620-626.
- 677 Mehrpooya, M., Sayyad, S. and Zonouz, M. J. 2017. "Energy, exergy and sensitivity analyses
678 of a hybrid combined cooling, heating and power (CCHP) plant with molten
679 carbonate fuel cell (MCFC) and Stirling engine." *Journal of Cleaner Production*, 148,
680 283-294.
- 681 Meiser, S., Schneider, S., Lüpfer, E., Schiricke, B. and Pitz-Paal, R. 2017. "Evaluation and
682 assessment of gravity load on mirror shape and focusing quality of parabolic trough
683 solar mirrors using finite-element analysis." *Applied Energy*, 185, 1210-1216.
- 684 Mohammadi, A. and Mehrpooya, M. 2016. "Exergy analysis and optimization of an
685 integrated micro gas turbine, compressed air energy storage and solar dish collector
686 process." *Journal of Cleaner Production*, 139, 372-383.
- 687 Omara, Z. and Eltawil, M. A. 2013. "Hybrid of solar dish concentrator, new boiler and simple
688 solar collector for brackish water desalination." *Desalination*, 326, 62-68.
- 689 Pavlović, S. R., Bellos, E. A., Stefanović, V. P., Tzivanidis, C. and Stamenković, Z. M. 2016.
690 "Design, simulation and optimization of a solar dish collector with spiral-coil thermal
691 absorber." *Thermal Science*(00), 104-104.
- 692 Prado, G. O., Vieira, L. G. M. and Damasceno, J. J. R. 2016. "Solar dish concentrator for
693 desalting water." *Solar Energy*, 136, 659-667.
- 694 Przenzak, E., Szubel, M. and Filipowicz, M. 2016. "The numerical model of the high
695 temperature receiver for concentrated solar radiation." *Energy Conversion and
696 Management*, 125, 97-106.
- 697 Reddy, K. and Kumar, N. S. 2009. "An improved model for natural convection heat loss from
698 modified cavity receiver of solar dish concentrator." *Solar Energy*, 83(10), 1884-
699 1892.
- 700 Reddy, K., Natarajan, S. K. and Veershetty, G. 2015. "Experimental performance
701 investigation of modified cavity receiver with fuzzy focal solar dish concentrator."
702 *Renewable Energy*, 74, 148-157.
- 703 Reddy, K. and Veershetty, G. 2013. "Viability analysis of solar parabolic dish stand-alone
704 power plant for Indian conditions." *Applied energy*, 102, 908-922.
- 705 Sánchez, D., Bortkiewicz, A., Rodríguez, J. M., Martínez, G. S., Gavagnin, G. and Sánchez,
706 T. 2016. "A methodology to identify potential markets for small-scale solar thermal
707 power generators." *Applied Energy*, 169, 287-300.
- 708 Tao, Y., He, Y., Cui, F. and Lin, C. 2013. "Numerical study on coupling phase change heat
709 transfer performance of solar dish collector." *Solar Energy*, 90, 84-93.
- 710 Xiao, G., Yang, T., Ni, D., Cen, K. and Ni, M. 2017. "A model-based approach for optical
711 performance assessment and optimization of a solar dish." *Renewable Energy*, 100,
712 103-113.
- 713 Zhu, X. W., Zhu, L. and Zhao, J. Q. 2017. "An in-depth analysis of conjugate heat transfer
714 process of impingement jet." *International Journal of Heat and Mass Transfer*, 104,
715 1259-1267.

716